Modeling The Sport Differential Mechanism

Maksym Diachuk [1] and Said M. Easa[1*]

[1] Department of Civil Engineering, Ryerson University, 350 Victoria Street, Toronto, ON M5B2K3, Canada; maksym.diachuk@ryerson.ca
* Corresponding author: seasa@ryerson.ca.

Abstract. The study is devoted to the issues of mathematical modeling and simulating the sport differential mechanism (DM) with controllable torque redistribution. The issue is caused by the elaboration of ADAS systems with the automated torque vectoring for transmissions of all-wheel-drive (AWD) vehicles and the inclusion of such devices in the combined autonomous vehicle trajectory control scheme. At the article's beginning, the use of devices for redistributing traction forces is reasoned by analyzing the curvilinear vehicle motion, where they could ensure the accuracy of vehicle steerability. The literature review highlights modern developments in the field of modeling and researching such DMs. Considering the vehicle turn with a minimum radius, the conditions corresponding to passing greater torque over the outrunning rear axle are determined. All the mechanism components and loads acting between them are described in detail. To form an original method of mathematical description of the mechanism functioning, the system of differential equations, systems of kinematic and force connections are considered separately. The article details the mathematical approach to generalize the way for automating the equation compilation for rotational mechanical systems such as vehicle transmissions. In the simulation section, a Simulink model reflecting the functional components and calculation procedures is presented. A series of testing and simulations on the DM operation with forcible torque distribution is carried out. Modeling data are presented, and the analysis of simulation results is performed. In the completion, conclusions are made regarding the scope and use of this model and the prospects for further developing the method proposed to automate the formation of equation systems.

Keywords: sport differential, torque vectoring, friction clutch, vehicle kinematics

1. Introduction

The integrated vehicle control affords maximum vehicle performance, handling accuracy, and safety given the intensive vehicle automation. Notably, the distributed torque technology for AWD vehicles provides the optimal mode for each wheel individually. In addition, it adjusts the exactness of the vehicle trajectory, which is especially essential for autonomous vehicles. Today, many vehicle manufacturers use the Sport Differential technology, which, unlike the pure torque vectoring (TV), does not require activating the inner wheels' brakes during curvilinear motion. Electric or hydraulic drives often carry out the control of such differentials. Simulation models

Preprints (www.preprints.org) | NOT PEER-REVIEWED | Posted: 26 November 2021 doi:10.20944/preprints202111.0507.v1

should be first elaborated, tested, and adjusted to help work with control algorithms for such mechanisms.

The characteristics of selected studies of vehicle differential mechanisms are presented in Table 1. It can be noted that the research field of differential mechanism (DM) models is quite broad, spanning different methods, approaches, and fields of study. Nevertheless, there is a specific lack of research on modeling active differentials with the electro-hydraulic drive since most papers have focused on handling an active limited-slip differential (ASLSD). Also, there is a lack of comprehensive studies that generalize the active differential control algorithms to solve the problems of motion stability, understeer compensation, and increase of vehicle passability. The math models and equation systems are primarily classic and do not imply systematization into one method. Some math models are too complicated to be used in vehicle dynamics and focused on pure mechanical objectives. The redistribution of traction forces contributes to reducing the lateral slip process due to partial compensation of lateral speeds, which increases control accuracy and motion stability.

Preprints (www.preprints.org) | NOT PEER-REVIEWED | Posted: 26 November 2021 doi:10.20944/preprints202111.0507.v1

57 Table 1. Characteristics of selected studies of vehicle differential mechanisms

Reference	Topic	Features
Gadola and Chindamo (2018)	Limited slip, self-locking TORSEN DM	- Actualize issues of differentials and their influence on vehicle dynamics. - Formed cornering moment in conditions of different slips. - Compared DM to the difference in angular speeds loading torques.
Morselli et al. (2006)	Convectional, LSD, controlled LSD	- Introduced torsional stiffness and lash of mechanical gearing. - Matrix approach and simulation schemes. - Developed detailed and simplified DM models. - Combined DM and vehicle modeling for testing the cornering effect.
Deur et al. (2010)	Active DM, TV	- Developed a unified math model for active differential dynamics. - Various DM designs and levels of model complexity are used. - Restricted applicability as estimated time response is needed.
Ji et al. (2011)	Active LSD (ALSD)	- Investigated driveline and tire model effects on the ALSD performance. - ALSD design includes friction clutches for transmitting the torque - Energy losses math models and Simulink tools are included.
Assadian et al. (2008)	Active LSD	- Developed a control algorithm for a rear-wheel-drive sport vehicle - Compared ALSD impact on vehicle model behavior. - Assessed ALSD influence on driver workload.
Annicchiarico et al. (2014)	Active LSD	- TV differential mechanism with electrohydraulic actuation. - Race car model with 7 DOFs and low ground effect. - Implemented nested control loop for the actuation system.
Jaafari and Shirazi (2018)	TV differential, electronic stability control	- Nonlinear vehicle model based on CarSim software. - TV Differential with two series of planetary gears. - Electronic stability model with three-layer Integrated control system. - Unscented Kalman filter and controller based on BA optimization.
Virlez et al. (2013)	TORSEN DM	- 3D cylindrical joint model with clearance, misalignment, and friction. - Matrix dynamics system including holonomic bi-lateral constraints.
Brumercik et al. (2015)	Inter-wheel differential	- DM with power balance and kinematic relations among three shafts. - Three differential equations; no efficiencies or changes in power flows.
Chen et al. (2017(1))	TV differential	- New TV differential based on a *Ravigneaux* gear set. - Two different speed ratios with only one pair of gear set. - *SimulationX* software is used to test maneuverability and steerability.
Chen et al. (2017(2))	Original DM design	- DM for TV concept; design combines inner gears. - Math model includes dynamics and kinematic constraints equations. - Losses, efficiencies, and power flow direction are neglected.
Forstinger et al. (2015)	Asymmetric differential	- Developed two DM variants (conic and planetary gear). - Dynamics and constraints; static friction and limited-slip functionality; - Overcomes simulation problems of discontinuity at zero angular speed.
Virlez et al. (2011)	TORSEN DM	- Multibody simulation using nonlinear FEM. - Flexible gear pair joints and contact conditions are used as constraints. - All-wheel-drive (AWD) model for estimating torque redistribution.
Russo et al. (2016)	Controllable DM	- DM based on the magnetorheological fluid to realize the locking state. - Torque, power balance, and kinematic constraint equations. - Double-controller scheme including extended Kalman filter. - Software-Hardware in the loop modeling with experimental prototype.

58

Preprints (www.preprints.org) | NOT PEER-REVIEWED | Posted: 26 November 2021 doi:10.20944/preprints202111.0507.v1

To actively control trajectory, simulation models must ensure the traction distribution on the physical level. Thus, the objective of this study is to develop and test a simulation model of the controlled sport differential for use in SIL/HIL modeling.

The research methodology shown in Fig. 1 explains the graduate steps needed to build the model. First, three types of equations on rotational motion should be considered separately. They reflect pure dynamics, kinematics, and force balance. Appending the equations for translationally moving elements, the math model of whole mechanism can be composed. A series of virtual tests foster to validate the sport differential's unique properties as well as simulation approach in general.

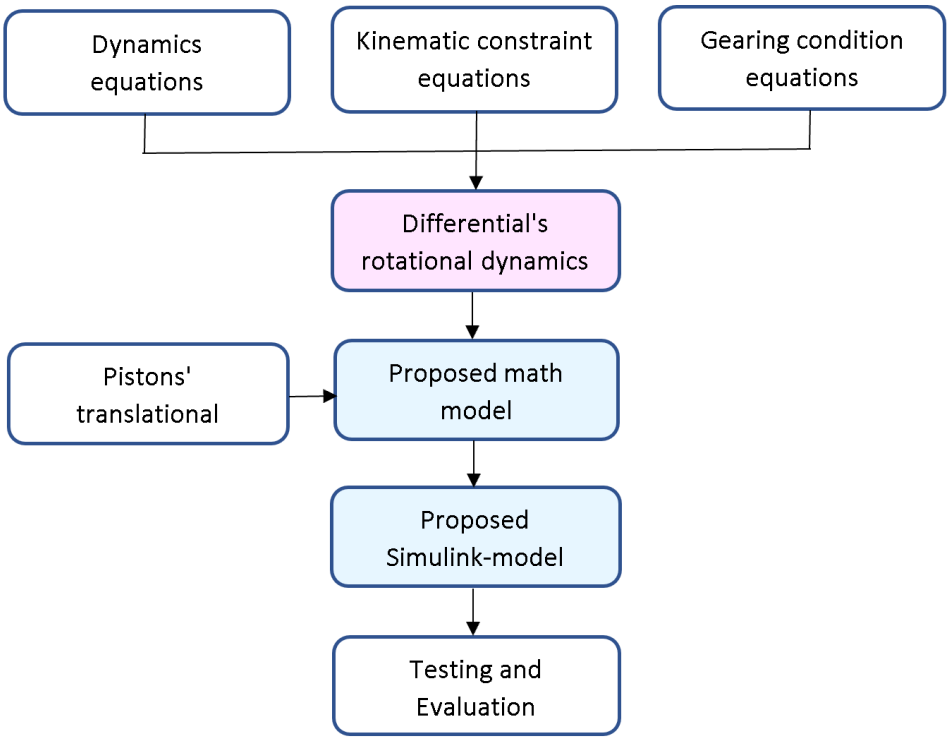

Figure. 1. Study methodology

3. Sport Differential Technology

3.1. Problem description

Consider the case of a passenger vehicle's curvilinear motion. It is almost impossible to ensure the ideal instant turn with the neutral steer in real conditions due to both tires' lateral elasticity and inevitable slip in the contact spots. As known well in this regard, two distinctive phenomena may occur - understeer and oversteer. Both processes are characterized by an intense lateral component of the instantaneous velocity in the tire-road contact spot, which is caused by the sideslip. These phenomena are associated with the distribution of vertical reactions along the vehicle axles. From a physical point of view, it is desirable to have approximately the same slip conditions for all tires to provide predictable control. Thus, AWD vehicles have an option for individually adjusting the traction forces to compensate the slip. If a vehicle is designed so that the front axle bears a larger mass, then it has the understeer tendency. In this case, as shown in Fig. 2a, the instantaneous rotation center O is located behind the rear axle. Thus, the transversal

Preprints (www.preprints.org) | NOT PEER-REVIEWED | Posted: 26 November 2021 doi:10.20944/preprints202111.0507.v1

components of the instantaneous velocities appear in all wheels' contact patches. The curvature of the motion trajectory decreases in comparison with the required one to ensure trajectory stability. As a result, to compensate for the lacking trajectory curvature, it is necessary to permanently increase the steered wheels' angles or reduce the cruise speed.

It is possible to create an additional yaw moment in the traction mode by changing longitudinal reactions on the vehicle sides' wheels. However, if symmetric (open) differentials are used in transmissions, the reactions on drive semi-axles are set practically equal, which does not affect the yaw moment. Thus, the prerequisites emerge for controlling the movement accuracy or tracking a planned trajectory by redistributing the torque between wheels, which may be achieved, among other things, by active differentials. Owing to setting the difference between traction forces on the same axle wheels, an additional yaw moment is occurred, decreasing the slip angles and approaching an instant turn to a scheme close to the neutral steer (Fig. 2b). At the same time, the tires' lateral forces can reach larger values and ensure control accuracy and trajectory stability (strict tracking) with a smaller steering angle.

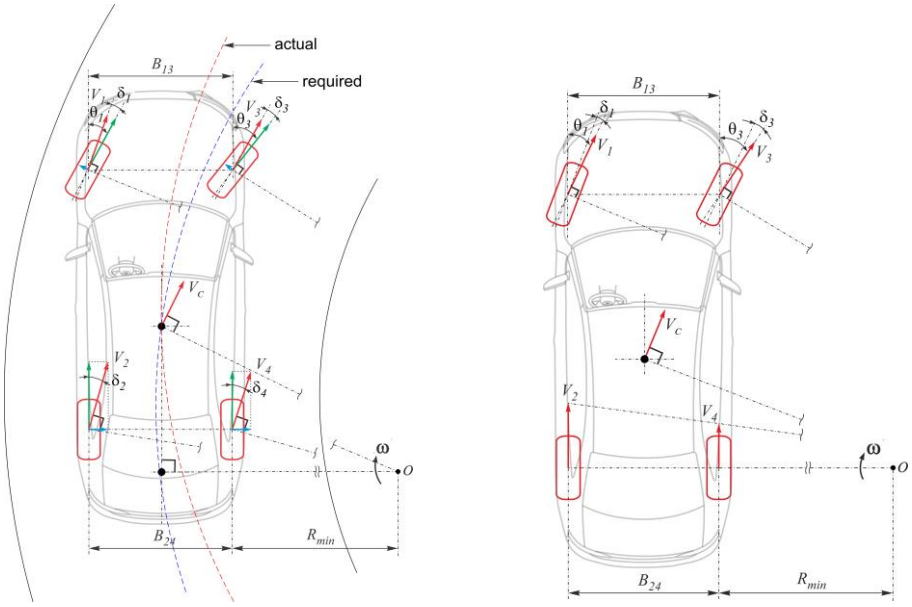

a) b)

Figure 2. Steerability cases: a - understeer, b - neutral steer

3.2. Differential's design

Several limited-slip differentials distribute the torques depending on the wheel operational mode. However, their redistribution concept implies that the greater torque is passed to a lagging wheel or with better adhesive conditions. The sport differential technology must transmit a larger torque value to an outrunning axle, which causes additional cornering (yaw moment) relative to the vertical axis passing through the mass center. Such a solution can be obtained using additional planetary gears (BMW, Honda) or, for example, two-step internal gearing (Audi) controlled by friction clutches with electric or hydraulic drives. Consider the design scheme and functioning of Audi Sport Differential (2021) shown in Fig. 3. The primary open information may be taken from Audi Sport Differential Technology (2021).

Preprints (www.preprints.org) | NOT PEER-REVIEWED | Posted: 26 November 2021 doi:10.20944/preprints202111.0507.v1

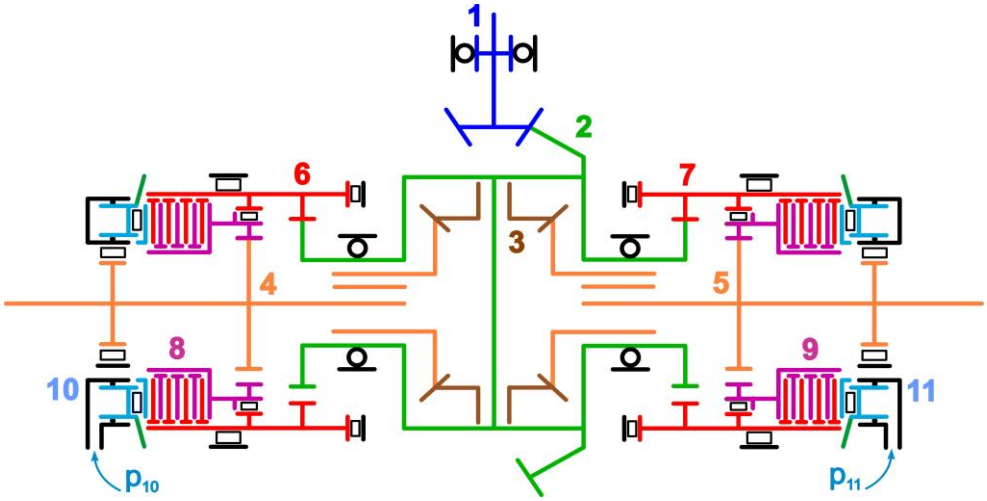

Figure 3. Scheme of Audi Sport Differential

The drive is carried out over the final gear pinion 1. The ring gear is rigidly connected to the differential carrier 2. Satellites 3, rotating around the axis fixed in the differential carrier, interact with side gears that drive the output axles 4 and 5 by the slots. The differential corps (carrier) has gear rims on the end sides for driving by internal gearing the coupling halves 6 and 7, in which rotational axes are respectively shifted relative to the carrier rotational axis. Using the frictional packs, the half-clutches 6 and 7 can drive the half-clutches 8 and 9, respectively, which are connected by an internal gearing to the output shafts 4 and 5. Toroidal hydraulic cylinders 10 and 11 are installed from each side to act on the clutch packs using the pressure p_{10} and p_{11}. Thus, by activating the required hydraulic cylinder, part of the carrier torque may be passed to the needed semi-axle using the frictional adhesion between the half-couplings over the two-step internal gearing.

Based on the sequence of links transmitting torque, the arrays of permanent liaisons ***L***, friction couples ***C***, vectors ***i*** of ratios and $\boldsymbol{\eta}_G$ of gearing efficiencies can be introduced. Moreover, if the numbers of each detail couple are denoted as a column-vector $\boldsymbol{L}_k$ (where $k = 1…m$, m – number of pairs), the sequential disposition of the conjugate details may be rearranged in a row vector ***l***.

$$\boldsymbol{L} = \begin{pmatrix} 1 & 2 & 2 & 2 & 3 & 3 & 4 & 5 \\ 2 & 3 & 6 & 7 & 4 & 5 & 8 & 9 \end{pmatrix},\ \boldsymbol{l} = (\boldsymbol{L}_1^T \quad \cdots \quad \boldsymbol{L}_m^T),\ \boldsymbol{C} = \begin{pmatrix} 6 & 7 \\ 8 & 9 \end{pmatrix} \tag{1}$$

$$\boldsymbol{i} = (i_{12} \quad i_{23} \quad i_{26} \quad i_{27} \quad i_{34} \quad i_{35} \quad i_{48} \quad i_{59})^T,$$

$$\boldsymbol{\eta}_G = (\eta_{12} \quad \eta_{23} \quad \eta_{26} \quad \eta_{27} \quad \eta_{34} \quad \eta_{35} \quad \eta_{48} \quad \eta_{59})^T \tag{2}$$

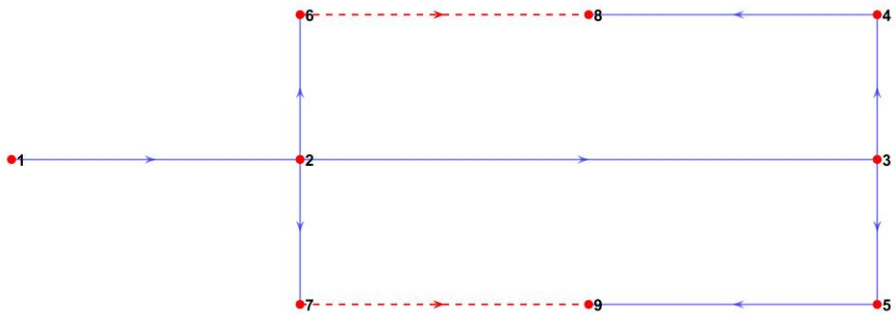

Preprints (www.preprints.org) | NOT PEER-REVIEWED | Posted: 26 November 2021 doi:10.20944/preprints202111.0507.v1

Figure 4. Graph of mechanical links

The friction clutch's slip degree affects the amount of additional torque withdrawn from the differential carrier, as well as the fact that, as shown in Fig. 2, for the general case of curvilinear motion, the angular speeds of the coupling halves 6, 7 and 8, 9 should be different. Thus, the pressure in the hydraulic cylinders must be adjusted in order, on the one hand, to maintain the ratio of wheels' angular speeds required during curvilinear motion and, on the other hand, to prevent the clutch lock-up. Requirements for passing the greater torque and high revolutions to the external wheel impose specific gearing ratios on the clutches 6-8 and 7-9. Consider this situation using the example of parameters in Fig. 2b, which corresponds to ideal cornering with minimal sideslip. Assuming that a clutch state close to complete locking is possible only for the variant of turning with a minimal radius, it is possible to determine the gear ratios for the drive of clutches' half-couplings. Determine the difference in angular speeds of the rear axle wheels. Their linear speeds are given by

$$V_4 = \omega R_{min}, \qquad V_2 = \omega(R_{min} + B_{24}) \tag{3}$$

where ω - instantaneous angular rate of the turn, B_{24} - transversal base of rear wheels. Then, the rear wheels' angular speeds ω_{w4}, ω_{w2} can be tied with parameters of the turn kinematics

$$\omega_{w4} = \frac{V_4}{r_{e4}} = \frac{\omega R_{min}}{r_{e4}}, \qquad \omega_{w2} = \frac{V_2}{r_{e2}} = \frac{\omega(R_{min}+B_{24})}{r_{e2}} \tag{4}$$

where r_{e4}, r_{e2} - wheels' effective radii (in most cases about the same).

The angular velocities' ratio, considering the designations in Figs. 1 and 2, is estimated as

$$k_\omega = \frac{\omega_{w2}}{\omega_{w4}} = \frac{\omega_4}{\omega_5} = \frac{\omega(R_{min}+B_{24})}{r_{w2}} \frac{r_{w4}}{\omega R_{min}} \approx \frac{R_{min}+B_{24}}{R_{min}} \tag{5}$$

where $\omega_{w2} = \omega_4$, $\omega_{w4} = \omega_5$ as the angular velocities of rear wheels (Fig. 2b) and the corresponding axles (Fig. 3).

For the case of the angular speed distribution based on the symmetric differential's kinematics (components 2, 3 in Fig. 3), the condition must be satisfied:

$$2\omega_2 = \omega_{w2} + \omega_{w4} = \omega_{w2} + \omega_{w2}/k_\omega = (1 + 1/k_\omega)\omega_{w2}$$
$$\text{but as well} \tag{6}$$
$$2\omega_2 = \omega_4 + \omega_5 = \omega_4 + \omega_4/k_\omega = (1 + 1/k_\omega)\omega_4$$

Then, the required angular speed of the differential carrier

$$\omega_2 = \frac{(1+1/k_\omega)}{2}\omega_4 = \frac{(1+1/k_\omega)}{2}\omega_{w2} \tag{7}$$

This determines the needed ratio between the steps of the half-couplings when they are locked by a friction clutch, that is

$$i_{24} = \frac{\omega_2}{\omega_4} = i_{26}i_{84} = \frac{\omega_2}{\omega_6}\frac{\omega_8}{\omega_4} = \frac{(1+1/k_\omega)}{2} \tag{8}$$

Since the torque is transmitted over the friction clutch in two steps of internal gearing, then

$$i_{26} = \omega_2/\omega_6 = z_6/z_2, \qquad i_{84} = \omega_8/\omega_4 = z_4/z_8 = 1/i_{48} \tag{9}$$

Preprints (www.preprints.org) | NOT PEER-REVIEWED | Posted: 26 November 2021 doi:10.20944/preprints202111.0507.v1

Taking integer teeth numbers for the gear rims of half-couplings, obtain the final values summarized in Tab. 2.

Table 2. Data for determining ratios for gears of half-couplings

B_{24}	R_{min}	i_{24}	z_2	z_6	i_{26}	z_4	z_8	i_{84}
1.551	5.8	0.887	33	41	1.242	25	35	0.714

The obtained value i_{24} shows that the difference between the angular speeds of the differential's carrier and the outer rear wheel differs only by about 11% even at the maximum steering angle. Thus, the angular speeds of half-couplings can be compared when moving with lesser curvature.

$$\omega_6 = \frac{\omega_2}{i_{26}} = \frac{\omega_2}{1.242} = 0.805\omega_2, \qquad \omega_8 = \omega_4 i_{84} = 0.714\omega_4 \tag{10}$$

If, for instance, the movement is close to a straight line, then $\omega_2 = \omega_4$, and it follows from Eq. (10) $\omega_6 > \omega_8$ by about 11%. Obviously, for all cases when the instantaneous curvature radius is greater than R_{min}, it remains true that $\omega_6 > \omega_8$, which corresponds to the need for friction clutch's slip that regulates the required instantaneous radius of the vehicle turn. In this case, half-couplings 6 or 7 will be driving, depending on the activation order. It is also evident that at turning with the maximum angles of steered wheels, $\omega 6 \approx \omega 8$ and consequently, the friction clutch can be locked. As it follows, if the pressure in the hydraulic cylinder leads to locking the clutch, then the ratio of the rear wheels' angular speeds will correspond to the kinematics of turning with a minimum radius even for straight motion.

4. Dynamics of design components of the Audi sport differential

Each structural component can be described by a system of equations, including dynamics balance, kinematic constraints, and contact force relations. Fig. 5 depicts all the design elements accompanied with the needed geometric parameters and force factors acting between the details.

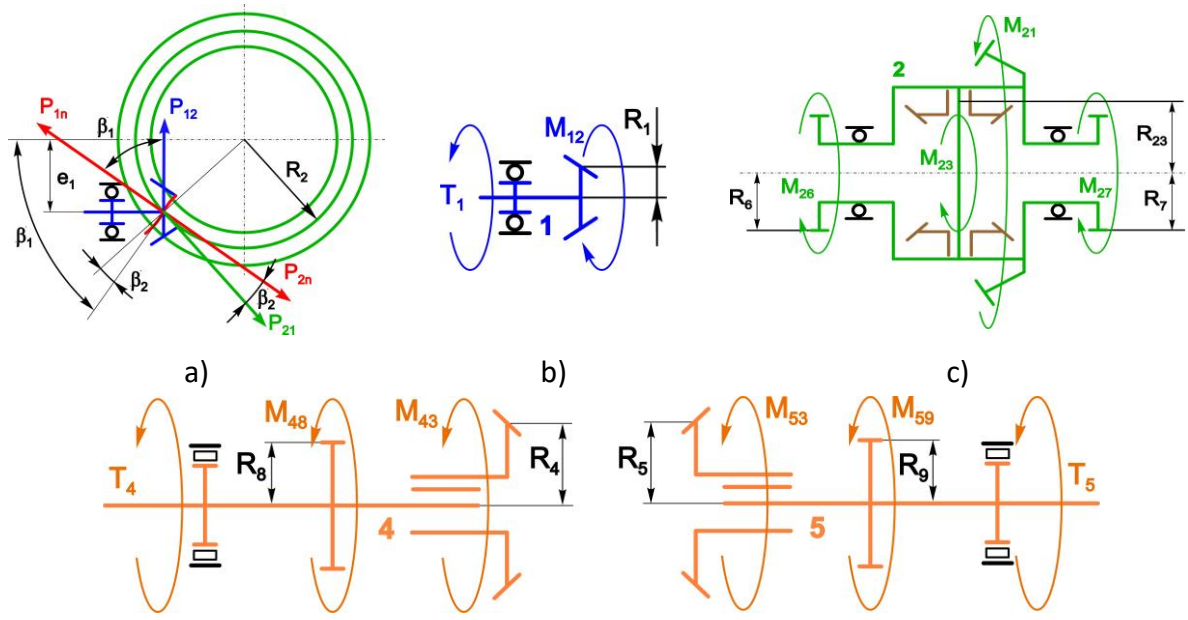

Preprints (www.preprints.org) | NOT PEER-REVIEWED | Posted: 26 November 2021 doi:10.20944/preprints202111.0507.v1

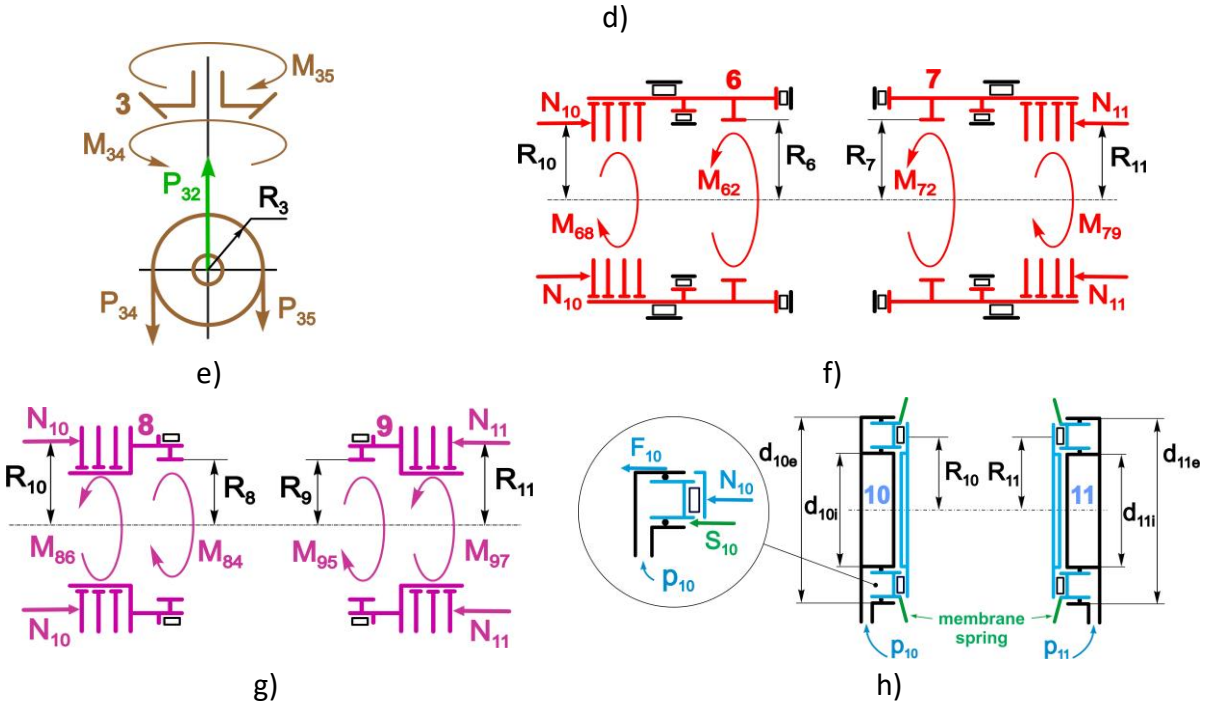

Figure 5. Parameters and force factors acting on the parts of the sport differential

4.1. Final drive

The rear axle final drive as the component of Audi Sport Differential is represented by the hypoid gearing, unlike, for instance, pure conic final drive of the vehicle front axle, and shown in Fig. 4a. Among the advantages of such a design solution, many aspects may be listed, such as a higher gear ratio with smaller gear ring size, increased teeth strength, and reduced noise. The main drawbacks include working with teeth sliding that reduces the gearing efficiency and requires special oils for high-pressure mechanical contacts. According to the scheme in Fig. 4a, the force of contact reaction may be decomposed as

$$P_{21} = P_n\, cos(\beta_1),\ P_{12} = P_n\, cos(\beta_2) \tag{11}$$

where angles β_1, β_2 are conditioned by the eccentricity e_1 and teeth curvature. It is recommended β_1 = 45…50°, β_2 = 45…50°.

Thus, the hypoid final drive ratio can be expressed as

$$i_{12} = \frac{\omega_1}{\omega_2} = \frac{M_{21}}{M_{12}} = \frac{D_\omega P_{12}}{d_\omega P_{21}} = \frac{D_\omega P_n\, cos(\beta_2)}{d_\omega P_n\, cos(\beta_1)} = \frac{D_\omega}{d_\omega} k_{12},\quad k_{12} = \frac{cos(\beta_2)}{cos(\beta_1)} = 1.2 \ldots 1.5 \tag{12}$$

where d_ω, D_ω – reference (pitch) diameters of pinion and ring correspondingly.

The hypoid gearing efficiency and teeth sliding speed may be calculated as

$$\eta_{12} = \frac{1+\mu_{12}\, tan(\beta_2)}{1+\mu_{12}\, tan(\beta_1)},\qquad v_s = v_1 \frac{\sin(\beta_1-\beta_2)}{\sin(\beta_2)} \tag{13}$$

where μ_{12} - coefficient of teeth friction (μ_{12} = 0.05…0.1, η_{12} = 0.96…0.97), v_1 - pinion peripheral speed.

Consequently, the torque relation for the final drive gearing may be written for two cases depending on the power flow passing through pinion and gear ring.

Preprints (www.preprints.org) | NOT PEER-REVIEWED | Posted: 26 November 2021 doi:10.20944/preprints202111.0507.v1

$$M_{21} + M_{12} i_{12} \eta_{12} = 0, \qquad M_{21} \eta_{21} + M_{12} i_{12} = 0 \tag{14}$$

4.2. Generalization of dynamics equations

4.2.1. System of rotational equations

Using Fig. 5, the system of differential equations can be combined for each design element, considering generalized states of power flows between the parts. Assuming the internal moments to be unknown, the system may be represented in the form of the extended left side, then

$$\begin{cases} I_1 \varepsilon_1 \eta_{1B} - M_{12} \eta_{1B}^{(c)} = T_1 \eta_{1B}^{(s)} + V_1 \\ I_2 \varepsilon_2 \eta_{2B} - M_{21} \eta_{2B}^{(s)} - M_{23} \eta_{2B}^{(c)} - M_{26} - M_{27} = V_2 \\ n_s I_3 \varepsilon_3 \eta_{3B} - n_s M_{34} \eta_{3B} - n_s M_{35} \eta_{3B} = n_s V_3 \\ I_4 \varepsilon_4 \eta_{4B} - M_{43} \eta_{4B}^{(s)} - M_{48} = T_4 \eta_{4B}^{(c)} + V_4 \\ I_5 \varepsilon_5 \eta_{5B} - M_{53} \eta_{5B}^{(s)} - M_{59} = T_5 \eta_{5B}^{(c)} + V_5 \\ I_6 \varepsilon_6 \eta_{6B} - M_{62} \eta_{6B}^{(s)} = M_{68} \eta_{6B}^{(c)} + V_6 \\ I_7 \varepsilon_7 \eta_{7B} - M_{72} \eta_{7B}^{(s)} = M_{79} \eta_{7B}^{(c)} + V_7 \\ I_8 \varepsilon_8 \eta_{8B} - M_{84} \eta_{8B}^{(s)} = M_{86} \eta_{8B}^{(c)} + V_8 \\ I_9 \varepsilon_9 \eta_{9B} - M_{95} \eta_{9B}^{(s)} = M_{97} \eta_{9B}^{(c)} + V_9 \end{cases} \tag{15}$$

where I_n – moment of inertia, ε_n – angular acceleration, η_{nB} – bearing efficiency, M_{nk} – internal and external moments (k – position of counteracting element), V_n – moment of viscous losses, T_n – external torque, n_s – number of satellites, n – position of element (n = {1…9}), s, c – upper indexes meaning state/converse state of transmitting the power.

Denote vectors: $\boldsymbol{I}$ – of inertias, $\boldsymbol{\eta}_B$ – of pure bearing efficiencies, $\boldsymbol{\eta}_T$ - of external torques' efficiencies, $\boldsymbol{\eta}_M$ – of friction torques' efficiencies, $\boldsymbol{n}_s$ – of satellite quantity.

$$\boldsymbol{I} = \begin{pmatrix} I_1 \\ I_2 \\ I_3 \\ I_4 \\ I_5 \\ I_6 \\ I_7 \\ I_8 \\ I_9 \end{pmatrix}, \quad \boldsymbol{\eta}_B = \begin{pmatrix} \eta_{1B} \\ \eta_{2B} \\ \eta_{3B} \\ \eta_{4B} \\ \eta_{5B} \\ \eta_{6B} \\ \eta_{7B} \\ \eta_{8B} \\ \eta_{9B} \end{pmatrix}, \quad \boldsymbol{\eta}_T = \begin{pmatrix} \eta_{1B}^{(s)} \\ 1 \\ 1 \\ \eta_{4B}^{(c)} \\ \eta_{5B}^{(c)} \\ 1 \\ 1 \\ 1 \\ 1 \end{pmatrix}, \quad \boldsymbol{\eta}_M = \begin{pmatrix} 1 \\ 1 \\ 1 \\ 1 \\ 1 \\ \eta_{6B}^{(c)} \\ \eta_{7B}^{(c)} \\ \eta_{8B}^{(c)} \\ \eta_{9B}^{(c)} \end{pmatrix}, \quad \boldsymbol{n}_s = \begin{pmatrix} 1 \\ 1 \\ n_s \\ 1 \\ 1 \\ 1 \\ 1 \\ 1 \\ 1 \end{pmatrix} \tag{16}$$

Then, it can be denoted for the matrix $\boldsymbol{I}_D$ of inertia influence

$$\boldsymbol{I}_D = diag(\boldsymbol{I})\, diag(\boldsymbol{n}_s)\, diag(\boldsymbol{\eta}_B) \tag{17}$$

4.2.2. Power flows and efficiencies

The states (s) and (c) are mutually opposite and caused by different events for various design elements. Thus, the main linked components of the differential k = {1, 2, 4, 5} can transmit the

Preprints (www.preprints.org) | NOT PEER-REVIEWED | Posted: 26 November 2021 doi:10.20944/preprints202111.0507.v1

direct (d) and reverse (r) power flow relative to the order of nodes in the vector $\boldsymbol{L}$, and, consequently, the possible states correspond to the combinations

$$\eta_{kB}^{(s)} \in \{\eta_{kB}^{(d)}, \quad \eta_{kB}^{(r)}\}, \qquad \eta_{kB}^{(c)} \in \{\eta_{kB}^{(r)}, \quad \eta_{kB}^{(d)}\}, \tag{18}$$

That is, if the state (s) is switched to (d), then state (c) is shifted to (r), and vice versa. In turn, the substitution of values is carried out according to the principle:

$$\eta_{kB}^{(s)} = \eta_{kB}^{(d)} = \eta_{kB} \Longrightarrow \eta_{kB}^{(c)} = \eta_{kB}^{(r)} = 1, \quad \eta_{kB}^{(s)} = \eta_{kB}^{(r)} = 1 \Longrightarrow \eta_{kB}^{(c)} = \eta_{kB}^{(d)} = \eta_{kB} \tag{19}$$

When considering the power flow, the direction may be determined from the following prerequisites. If the power is transmitted through the drivetrain to wheels, the input flow must exceed the algebraic sum of the output power flows regardless of the internal mechanism state since the mechanical connections themselves already take into account the ratio of the input and output powers. Then, the direct power flow corresponds to the condition

$$|T_1\omega_1| > |T_4\omega_4 + T_5\omega_5| \tag{20}$$

which means the state (s) has been switched to the (d).

On the other hand, if the wheels drive the semi-axles, the power is returned to the transmission and the flow becomes reverse. Another situation is tied with redistributing the external powers between wheels when their signs are opposite and modules differ slightly. In these cases, the condition is

$$|T_4\omega_4 + T_3\omega_3| \geq |T_1\omega_1| \tag{21}$$

which corresponds to switching state (s) to (r).

There is a different picture with the drive of the friction clutches' components corresponding to the elements k = {6, 7, 8, 9}. In this case, in each element, the direct/reverse state can be changed independently of the general power flow direction. That is, states (s) and (c) can take on direct and reverse modes (d) and (r) depending on whether a flow corresponds to the direct order of nodes while transmitting power or to the reverse order (Fig. 4). Thus, the math approach, in this case, is equal to Eq. (19).

Note that each friction clutch can be activated individually, withdrawing some torque from the carrier as well as returning to it. Elements k = {6, 7} are initially in the direct phase, transmitting torques from the carrier even in the case of disengaged clutches. In this case, the condition for transmitting power from the carrier can be represented as

$$|M_{62}| - |M_{86}| > 0, \qquad |M_{72}| - |M_{97}| > 0 \tag{22}$$

Elements k = {8, 9} are initially in the passive phase (idle). The condition for activating the additional torque on a semi-axle can be expressed as

$$|M_{86}| - |M_{84}| > 0, \qquad |M_{97}| - |M_{95}| > 0 \tag{23}$$

Values M_{86}, M_{97} are calculated by the dependencies for frictional moments to be considered below.

Denote vectors of all the internal moments $\boldsymbol{M}$, $\boldsymbol{N}_s$ of satellite quantity, bearing efficiencies depending on states: $\boldsymbol{\eta}_{BM}$ of internal links, $\boldsymbol{\eta}_{BS}$ of satellites, $\boldsymbol{\eta}_{BC}$ of clutches. Vector $\boldsymbol{N}_s$ can be

Preprints (www.preprints.org) | NOT PEER-REVIEWED | Posted: 26 November 2021 doi:10.20944/preprints202111.0507.v1

obtained by changing values in vector $\boldsymbol{l}$ Eq. (1) with 1, except for positions equal to numeric 3 (satellites), which are replaced with the number of satellites n_s. Vector $\boldsymbol{\eta}_{BS}$ structurally corresponds to the vector $\boldsymbol{N}_s$ but contains efficiency η_{3B} instead of n_s.

$$\boldsymbol{M} = \begin{pmatrix} M_{12} \\ M_{21} \\ M_{23} \\ M_{32} \\ M_{26} \\ M_{62} \\ M_{27} \\ M_{72} \\ M_{34} \\ M_{43} \\ M_{35} \\ M_{53} \\ M_{48} \\ M_{84} \\ M_{59} \\ M_{95} \end{pmatrix}, \quad \boldsymbol{N}_s = \begin{pmatrix} 1 \\ 1 \\ 1 \\ n_s \\ 1 \\ 1 \\ 1 \\ 1 \\ n_s \\ 1 \\ n_s \\ 1 \\ 1 \\ 1 \\ 1 \\ 1 \end{pmatrix}, \quad \boldsymbol{\eta}_{BM} = \begin{pmatrix} \eta_{1B}^{(c)} \\ \eta_{2B}^{(s)} \\ \eta_{2B}^{(c)} \\ 1 \\ 1 \\ 1 \\ 1 \\ 1 \\ 1 \\ \eta_{4B}^{(s)} \\ 1 \\ \eta_{5B}^{(s)} \\ 1 \\ 1 \\ 1 \\ 1 \end{pmatrix}, \quad \boldsymbol{\eta}_{BS} = \begin{pmatrix} 1 \\ 1 \\ 1 \\ \eta_{3B} \\ 1 \\ 1 \\ 1 \\ 1 \\ \eta_{3B} \\ 1 \\ \eta_{3B} \\ 1 \\ 1 \\ 1 \\ 1 \\ 1 \end{pmatrix}, \quad \boldsymbol{\eta}_{BC} = \begin{pmatrix} 1 \\ 1 \\ 1 \\ 1 \\ 1 \\ \eta_{6B}^{(s)} \\ 1 \\ \eta_{7B}^{(s)} \\ 1 \\ 1 \\ 1 \\ 1 \\ 1 \\ \eta_{8B}^{(s)} \\ 1 \\ \eta_{9B}^{(s)} \end{pmatrix} \tag{24}$$

Matrix $\boldsymbol{H}_B$ is obtained based on vectors $\boldsymbol{\eta}_{BM}$, $\boldsymbol{\eta}_{BS}$, and $\boldsymbol{\eta}_{BC}$, and $\boldsymbol{H}_T$ by using $\boldsymbol{\eta}_T$ and $\boldsymbol{\eta}_M$

$$\boldsymbol{H}_B = diag(\boldsymbol{\eta}_{BM})diag(\boldsymbol{\eta}_{BS})diag(\boldsymbol{\eta}_{BC}), \qquad \boldsymbol{H}_T = diag(\boldsymbol{\eta}_T)diag(\boldsymbol{\eta}_M) \tag{25}$$

4.2.3. Internal moments

Suppose that the vector $\boldsymbol{M}$ components are initially unknown, which allows us to consider them on the system's left side (15). Each pair M_{kl}, M_{lk} reflects the force interaction of conjugated parts. To group the moments according to the corresponding equations, a logical matrix $\boldsymbol{E}$ may be introduced. To obtain it, the element-wise comparison of two matrices should be carried out. One matrix is obtained by repeating the column-vector of the parts' serial numbers (1 ... n) the number of times corresponding to the doubled number ($2{\cdot}m$) of connections in the matrix $\boldsymbol{L}$. The second matrix is obtained by repeating the row-vector l from Eq. (1) the number of times equal to the number of details (n). However, the pair 2-3 does not provide an absolute kinematic connection between the carrier and the satellites. The moments act in different planes, so the element corresponding to row 3 and column 2·2 = 4 must be zeroed in matrix $\boldsymbol{E}$. Thus, the left part of the system Eq. (15) associated with unknown moments may be represented in the matrix form as

$$\boldsymbol{E}_D = -\boldsymbol{E}\, diag(\boldsymbol{N}_s)\, diag(\boldsymbol{H}_B) \tag{26}$$

4.2.4. Loading conditions and viscous resistance

Introducing the vectors $\boldsymbol{v}$ of viscous resictance coefficients, $\boldsymbol{V}$ of viscous moments, $\boldsymbol{\omega}_h$ of housing angular speeds, and $\boldsymbol{\omega}_r$ of relative angular speeds, then

Preprints (www.preprints.org) | NOT PEER-REVIEWED | Posted: 26 November 2021 doi:10.20944/preprints202111.0507.v1

$$\boldsymbol{v} = \begin{pmatrix} v_1 \\ v_2 \\ v_3 \\ v_4 \\ v_5 \\ v_6 \\ v_7 \\ v_8 \\ v_9 \end{pmatrix}, \ \boldsymbol{V} = \begin{pmatrix} V_1 \\ V_2 \\ V_3 \\ V_4 \\ V_5 \\ V_6 \\ V_7 \\ V_8 \\ V_9 \end{pmatrix}, \ \boldsymbol{\omega}_h = \begin{pmatrix} 0 \\ 0 \\ 0 \\ \omega_2 \\ \omega_2 \\ 0 \\ 0 \\ \omega_6 \\ \omega_7 \end{pmatrix}, \ \boldsymbol{\omega}_r = \boldsymbol{\omega} - \boldsymbol{\omega}_h, \ \boldsymbol{V} = -diag(\boldsymbol{v})\boldsymbol{\omega}_r \tag{27}$$

Consequently, the viscous losses for the system of Eq. (15)

$$\boldsymbol{V}_D = diag(\boldsymbol{n}_s)\boldsymbol{V} = -diag(\boldsymbol{n}_s)\, diag(\boldsymbol{v})\, \boldsymbol{\omega}_r \tag{28}$$

Introduce vectors $\boldsymbol{T}$ of external torques, $\boldsymbol{T}_T$ of the known external torques, and matrix $\boldsymbol{e}_T$ of transition to the vector $\boldsymbol{T}$, then

$$\boldsymbol{T} = \begin{pmatrix} T_1 \\ 0 \\ 0 \\ T_4 \\ T_5 \\ M_{68} \\ M_{79} \\ M_{86} \\ M_{97} \end{pmatrix}, \ \boldsymbol{T}_T = \begin{pmatrix} T_1 \\ T_4 \\ T_5 \\ M_{86} \\ M_{97} \end{pmatrix}, \ \boldsymbol{e}_T = \begin{pmatrix} 1 & 0 & 0 & 0 & 0 \\ 0 & 0 & 0 & 0 & 0 \\ 0 & 0 & 0 & 0 & 0 \\ 0 & 1 & 0 & 0 & 0 \\ 0 & 0 & 1 & 0 & 0 \\ 0 & 0 & 0 & -1 & 0 \\ 0 & 0 & 0 & 0 & -1 \\ 0 & 0 & 0 & 1 & 0 \\ 0 & 0 & 0 & 0 & 1 \end{pmatrix}, \ \boldsymbol{T} = \boldsymbol{e}_T\boldsymbol{T}_T \tag{29}$$

Consequently, the right part of the Eq. (xx) system may be represented in the matrix form

$$\boldsymbol{T}_D = \boldsymbol{H}_T\boldsymbol{T} = \boldsymbol{H}_T\boldsymbol{e}_T\boldsymbol{T}_T \tag{30}$$

Thus, the system of Eq. (15) may be written as

$$\boldsymbol{I}_D\boldsymbol{\varepsilon} + \boldsymbol{E}_D\boldsymbol{M} = \boldsymbol{T}_D + \boldsymbol{V}_D \tag{31}$$

4.3. Friction torque

4.3.1. Friction model

Additional delivery of a power flow in this DM design is carried out by the external control according to the necessity (dashed lines in Fig. 4) and corresponds to the interactions of nodes specified in the matrix $\boldsymbol{C}$ Eq. (1). The formation of driving moments in friction clutches is schematically shown in Fig. 5 f, g, h. Moreover, it is obvious that M_{68} = -M_{86}, M_{79} = -M_{97}, which allows to consider only driven parts. Frictional moments in clutches are functions of design parameters and normal forces N_{10}, N_{11}.

$$M_{kl} = f_{kl}N_pR_pn_{kl} \tag{32}$$

where M_{kl} – driving frictional moment, k = {8, 9} and l = {6, 7} – indexes denoting frictional elements, N_p – normal force, p = {10, 11} – indexes denoting pressing elements, R_p – average friction radius, f_{kl} – friction factor, n_{kl} – number of friction surfaces.

The hyperbolic tangent function can be accepted as a frictional model ensuring automatic changing the sign when clutch sliding. Also, this model usage is sufficient since the design does

not provide strict conditions for locking clutches, as it is required, for example, in the automatic gearbox. Moreover, the value of torque transmitted to a wheel should preferably be proportional to the pressure in a hydraulic cylinder, which makes the control predictable and stable.

$$f_{kl} = \mu_{kl}\, tanh(c_{kl}\Delta\omega_{kl}), \quad \Delta\omega_{kl} = (\omega_l - \omega_k) \tag{33}$$

where μ_{kl} - module value of friction coefficient, c_{kl} – intensity coefficient.

4.3.2. Clutch locking

Despite the possibility of conditionally unlimited increasing the normal force N_p in Eq. (32), the frictional moment is restricted by the critical value N_{pc} leading to locking a clutch. At the same time, a N_{pc} value does not remain constant being consistent with external loading changes. In this regard, it is necessary to provide an algorithm for setting the locking mode and limiting the friction torque. For this, introduce a threshold zone $\pm\Delta\omega_c$ in the vicinity of $\Delta\omega_{kl} = 0$, where the mode is equivalent to the lock state and the sliding is practically absent. The current value of the clutch compression force N_p can result two states:

$$|\Delta\omega_{kl}| > \Delta\omega_c, \quad |\Delta\omega_{kl}| \le \Delta\omega_c \tag{34}$$

If the absolute value of the relative angular speed does not exceed a threshold value, the N_p value is stored into the memory as $N_{p(-1)}$. At the next step, the new value $N_{p(+1)}$ be compared with the previous one for the minimum

$$N_p = min\,\{N_{p(-1)} \quad N_{p(+1)}\} \tag{35}$$

Note that an N_p value is not related to a friction moment sign. This point stipulates only positive values of N_p. The friction moment in this state is defined as

$$M_{kl} = \mu_{kl} N_p R_p n_{kl}\, sgn(\Delta\omega_{kl}) \tag{36}$$

When $\Delta\omega_{kl}$ exceeds a threshold value, the N_p current value is taken as the basic one and cycles are repeated again.

4.3.3. Normal force

Consider the translational motion of pistons compressing the clutches shown in Fig. 5h. The system of equations can be represented as

$$\begin{cases} dx_p/dt = s_p \\ m_p a_p = P_p + N'_p \end{cases} \tag{37}$$

where m_p – piston mass, a_p – piston acceleration, s_p - piston velocity, x_p - piston translational displacement, P_p – resulting piston force, N'_p - force of combined normal reaction, p – index of translational element (p = 10, 11).

Denote

$$P_p = p_p A_p + F_p + S_p \tag{38}$$

Where p_p – pressure in cylinder p, A_p – piston area, F_p - resistance force of interaction between cylinder and cuff, S_p - elastic force of return springs.

The components of Eq. (38) may be found by following formulas, considering p = 10, 11:

$$A_p = \frac{\pi}{4}\left(d_{pe}^2 - d_{pi}^2\right) \tag{39}$$

where d_{pe}, d_{pi} – piston external and internal diameters.

Preprints (www.preprints.org) | NOT PEER-REVIEWED | Posted: 26 November 2021 doi:10.20944/preprints202111.0507.v1

$$S_p = -k_{sp}\left(x_p + \Delta_{p0}\right) \tag{40}$$

where k_{sp} – spring stiffness, Δ_{p0} – initial deformation.

$$F_p = -\left(p_p h\pi\left(d_{pe} + d_{pi}\right)f_p + \nu_p s_p\right), \quad f_p = \mu_p \tanh\left(c_p s_p\right) \tag{41}$$

where h – cuff width, f_p – friction factor, ν_p – viscous coefficient, μ_p – module value of translational friction coefficient, c_p – intensity coefficient.

The simplest way to form the force N'_p consists of setting piecewise linear functions depending on the piston stroke. The N'_p reaction ensures the piston hard stop in the boundary positions, while the N_p component is the clutch compressing force.

$$N'_p = -k_{p1} x_p E_H\left(-x_p\right) - N_p,$$
$$N_p = k_{p2}\left(x_p - x_{p\Delta}\right)\left(E_H\left(x_p - x_{p\Delta}\right) - E_H\left(x_p - x_{h\Delta}\right)\right) + P_{po} E_H\left(x_p - x_{h\Delta}\right) \tag{42}$$

where k_{p1}, k_{p2} – stiffness of elastic forces in the piston boundary positions, $x_{p\Delta}$ - clearance for ensuring the complete clutch disengagement, $x_{h\Delta}$ – piston stroke corresponding to the hard-stop, P_{po} – value of the P_p force evaluated at preceding time-step, E_H – Heaviside step-function.

4.4. Kinematic connections and constraints

In describing the ideal kinematic connections adopted in the sport differential design, two moments occur regarding the continuity of links transmitting both absolute and relative kinematic parameters. Introduce the basic kinematic vectors

$$\boldsymbol{\omega} = \begin{pmatrix} \omega_1 \\ \vdots \\ \omega_n \end{pmatrix}, \qquad \boldsymbol{\varepsilon} = \frac{d\boldsymbol{\omega}}{dt} = \begin{pmatrix} \varepsilon_1 \\ \vdots \\ \varepsilon_n \end{pmatrix} \tag{43}$$

where $n = 9$ – number of rotating components.

Particularly, as shown in Fig. 3, some of the elements (2, 3, 4, 5) have differential relations, and the motion of the satellites 3 is described by the relative angular speed ω_3. Thus, for all couples (columns) of the matrix $\boldsymbol{L}$ Eq. (1), except for containing the element 3, the gear ratios are defined as

$$i_{kl} = \omega_k / \omega_l \tag{44}$$

where k = {1, 2, 2, 4, 5}, l = {2, 6, 7, 8, 9} – the positions of the couples' elements transmitting the absolute angular speeds.

In this case, the equation of continuity of a kinematic connection in general form can be written as

$$\omega_k - i_{kl}\omega_l = 0, \qquad \varepsilon_k - i_{kl}\varepsilon_l = 0 \tag{45}$$

In the case of differential dependency between links

$$i_{kl} = i_{kl}^{(p)} = \left(\omega_k - \omega_p\right)/\left(\omega_l - \omega_p\right) \tag{46}$$

where k = {4, 5}, l = {5, 4} – the positions of the couples' elements transmitting the relative angular speeds, p = {2, 2} – positions of the stopped carrier.

Preprints (www.preprints.org) | NOT PEER-REVIEWED | Posted: 26 November 2021 doi:10.20944/preprints202111.0507.v1

The general remark regarding the sign of a gear ratio can be made, assuming that it is determined depending on the rotational directions of the corresponding parts. Thus, if both linked parts provide the same counterclockwise and clockwise rotations, their gear ratio is to be considered as positive regardless of whether the engagement is external or internal. Conversely, a change of direction means a negative gear ratio. For example, the couple 3-5 (Fig. 3) ensures the rotation of the satellites 3 counterclockwise if the side gear 5 also rotates counterclockwise. But the symmetrical to it couple 3-4 ensures the clockwise rotation of the satellites 3 if the side gear 4 rotates counterclockwise, which corresponds to a negative gear ratio. Note that with this approach, the signs of the mechanism's force and kinematic gear ratios coincide.

As known, the differential mechanism provides two degrees of freedom, and at the same time, according to Fig. 3, three couples of details are involved. It is assumed that the ratios i_{34} and i_{35} correspond to when carrier 2 is stopped. Differential constraints are described by the Willis formula, which gives the following statements for the case of power distribution

$$i_{45}^{(2)} = \frac{\omega_4-\omega_2}{\omega_5-\omega_2} = \frac{\omega_4^{(2)}}{\omega_5^{(2)}} = \frac{\omega_4^{(2)}}{\omega_3}\frac{\omega_3}{\omega_5^{(2)}} = -\frac{z_3}{z_4}\frac{z_5}{z_3} = \frac{i_{43}^{(2)}}{i_{53}^{(2)}} = \frac{i_{35}}{i_{34}} \tag{47}$$

where z_3, z_5 – teeth numbers of corresponding elements.

The relative ratios between side gears and satellites are determined as follows

$$i_{43}^{(2)} = \frac{\omega_4-\omega_2}{\omega_3} = \frac{\omega_4^{(2)}}{\omega_3} = \frac{1}{i_{34}}, \quad i_{53}^{(2)} = \frac{\omega_5-\omega_2}{\omega_3} = \frac{\omega_5^{(2)}}{\omega_3} = \frac{1}{i_{35}} \tag{48}$$

These Eqs. (47, 48) give the relative kinematic expressions for differential links

$$\begin{gathered}(\omega_4-\omega_2)i_{34}-(\omega_5-\omega_2)i_{35}=0,\\ \omega_3-(\omega_4-\omega_2)i_{34}=0, \qquad \omega_3-(\omega_5-\omega_2)i_{35}=0\end{gathered} \tag{49}$$

Thus, the resulting system of algebraic equations of kinematic connections, using Eqs. (48, 49), is

$$\begin{cases} \varepsilon_1 - i_{12}\varepsilon_2 = 0 \\ (\varepsilon_4-\varepsilon_2)i_{34}-(\varepsilon_5-\varepsilon_2)i_{35}=0 \\ \varepsilon_2 - i_{26}\varepsilon_6 = 0 \\ \varepsilon_2 - i_{27}\varepsilon_7 = 0 \\ \varepsilon_3-(\varepsilon_4-\varepsilon_2)i_{34}=0 \\ \varepsilon_3-(\varepsilon_5-\varepsilon_2)i_{35}=0 \\ \varepsilon_4 - i_{48}\varepsilon_8 = 0 \\ \varepsilon_5 - i_{59}\varepsilon_9 = 0 \end{cases} \tag{50}$$

This system can be decomposed considering in Eqs. (1, 2) vector $\boldsymbol{i}$ and matrix $\boldsymbol{L}$

$$\boldsymbol{\varepsilon}_{in} = \begin{pmatrix}\varepsilon_1\\ \varepsilon_2\\ \varepsilon_2\\ \varepsilon_2\\ \varepsilon_3\\ \varepsilon_3\\ \varepsilon_4\\ \varepsilon_5\end{pmatrix}, \quad \boldsymbol{\varepsilon}_{out} = \begin{pmatrix}\varepsilon_2\\ \varepsilon_3\\ \varepsilon_6\\ \varepsilon_7\\ \varepsilon_4\\ \varepsilon_5\\ \varepsilon_8\\ \varepsilon_9\end{pmatrix} - \begin{pmatrix}0\\ 0\\ 0\\ 0\\ \varepsilon_2\\ \varepsilon_2\\ 0\\ 0\end{pmatrix}, \quad \boldsymbol{\varepsilon}_{in} = \boldsymbol{e}_{in}\boldsymbol{\varepsilon}, \quad \boldsymbol{\varepsilon}_{out} = \boldsymbol{e}_{out}\boldsymbol{\varepsilon} \tag{51}$$

Preprints (www.preprints.org) | NOT PEER-REVIEWED | Posted: 26 November 2021 doi:10.20944/preprints202111.0507.v1

The matrices $\boldsymbol{e}_{in}$, $\boldsymbol{e}_{out}$ can be obtained based on rows 1 and 2 of the matrix $\boldsymbol{L}$, respectively. For this, two matrices are logically compared, one of which is obtained by repeating an elements' column-vector several times equal to the number of connections, and the second - by copying a row of matrix *L* (upper for $\boldsymbol{e}_{in}$ or lower for $\boldsymbol{e}_{out}$) several times equal to the number of elements being considered (*n* in this case). The result will give logical matrices containing 0 and 1. Note that the link 2-3 in the matrix *L* describing the interaction between the carrier 2 and satellites 3 is differential, and therefore the corresponding row in the vectors $\boldsymbol{\varepsilon}_{in}$, $\boldsymbol{\varepsilon}_{out}$ must be zeroed and links 3-4 and 3-5 to be represented by relative angular accelerations following Eq. (49). To do this, introduce the matrix $\boldsymbol{e}_d$, which ensures the replacement of the conjugation of the carrier and satellites rotating in different planes with a differential connection by subtracting the angular accelerations for the side gears and satellites relative to the satellite. Thus, Eq. (50) in matrix form is

$$\boldsymbol{e}_\varepsilon = \boldsymbol{e}_d(\boldsymbol{e}_{in} - diag(\boldsymbol{i})\boldsymbol{e}_{out}), \quad \boldsymbol{e}_\varepsilon\boldsymbol{\varepsilon} = \boldsymbol{z} \tag{52}$$

where $\boldsymbol{z}$ – zero column-vector with the length corresponding to the number of kinematic links.

On the other hand, the differential is characterized by two degrees of freedom. That is, the vector $\boldsymbol{\varepsilon}$ of angular accelerations can be expressed through the vector $\boldsymbol{\varepsilon}_D$ containing only the angular accelerations of the side gears

$$\boldsymbol{\varepsilon}_D = \begin{pmatrix}\varepsilon_4\\ \varepsilon_5\end{pmatrix}, \qquad \boldsymbol{\varepsilon} = \boldsymbol{E}_\varepsilon\boldsymbol{\varepsilon}_D \tag{53}$$

where

$$\boldsymbol{E}_\varepsilon = \frac{1}{(i_{34}-i_{35})}\begin{pmatrix} i_{12}i_{34} & -i_{12}i_{35}\\ i_{34} & -i_{35}\\ -i_{35}i_{34} & i_{35}i_{34}\\ (i_{34}-i_{35}) & 0\\ 0 & (i_{34}-i_{35})\\ i_{34}/i_{26} & -i_{35}/i_{26}\\ i_{34}/i_{27} & -i_{35}/i_{27}\\ (i_{34}-i_{35})/i_{48} & 0\\ 0 & (i_{34}-i_{35})/i_{59}\end{pmatrix} \tag{54}$$

Thus, the substitution of Eq. (54) in Eq. (52) helps to reduce the number of unknown kinematic variables

$$\boldsymbol{e}_\varepsilon = \boldsymbol{e}_d(\boldsymbol{e}_{in} - diag(\boldsymbol{i})\boldsymbol{e}_{out}), \qquad \boldsymbol{e}_\varepsilon\boldsymbol{E}_\varepsilon\boldsymbol{\varepsilon}_D = \boldsymbol{z} \tag{55}$$

4.5. Gearing conditions

Consider the force factors emerging in conjugated components. In the general case, the sum of the moments at a node can be expressed as

$$M_k i_{kl} + M_l = 0 \tag{56}$$

where k, l – indexes of conjugated details, i_{kl} – ratio.

Note that in the general case, i_{kl} can be both positive and negative depending on whether the connection changes the moment sign. Thus, for example, for an internal gearing pair, the

directions of positive moments coincide and, therefore, the gear ratio is positive, which determines the opposite signs of M_l and M_k as the driving and reaction moments in a node.

Assuming that a part of mechanical energy is lost during transmitting the moment, for the cases of direct and reverse power flow, it can be respectively written

$$M_{kl} i_{kl} \eta_{kl} + M_{lk} = 0, \qquad M_{kl} i_{kl} + M_{lk} \eta_{lk} = 0 \tag{57}$$

where η_{kl}, η_{lk} – direct and reverse gearing efficiencies, correspondingly (it may be supposed $\eta_{kl} = \eta_{lk}$).

Denote vectors of gearing efficiencies $\boldsymbol{\eta}_G$ for exceptionally differential's details, of gearing efficiencies $\boldsymbol{\eta}_C$ for clutches' details, and of unknown internal moments $\boldsymbol{M}_D$

$$\boldsymbol{\eta}_G^{(s)} = \begin{pmatrix} \eta_{12}^{(s)} \\ \eta_{23}^{(s)} \\ 1 \\ 1 \\ \eta_{34}^{(s)} \\ \eta_{35}^{(s)} \\ 1 \\ 1 \end{pmatrix}, \quad \boldsymbol{\eta}_G^{(c)} = \begin{pmatrix} \eta_{12}^{(c)} \\ \eta_{23}^{(c)} \\ 1 \\ 1 \\ \eta_{34}^{(c)} \\ \eta_{35}^{(c)} \\ 1 \\ 1 \end{pmatrix}, \quad \boldsymbol{\eta}_C^{(s)} = \begin{pmatrix} 1 \\ 1 \\ \eta_{26}^{(s)} \\ \eta_{27}^{(s)} \\ 1 \\ 1 \\ \eta_{48}^{(s)} \\ \eta_{59}^{(s)} \end{pmatrix}, \quad \boldsymbol{\eta}_C^{(c)} = \begin{pmatrix} 1 \\ 1 \\ \eta_{26}^{(c)} \\ \eta_{27}^{(c)} \\ 1 \\ 1 \\ \eta_{48}^{(c)} \\ \eta_{59}^{(c)} \end{pmatrix}, \quad \boldsymbol{M}_D = \begin{pmatrix} M_{21} \\ M_{32} \\ M_{62} \\ M_{72} \\ M_{43} \\ M_{53} \\ M_{84} \\ M_{95} \end{pmatrix} \tag{58}$$

where s, c – upper indexes for determining possible state/converse state efficiencies depending on whether the power is being transmitted according to the order of nodes in matrices $\boldsymbol{L}$ and $\boldsymbol{C}$ or conversely.

Thus, the systems of moments' equilibrium for the generalized case of direct or reverse power flow is

$$\begin{cases} M_{21}\eta_{12}^{(c)} + M_{12}\eta_{12}^{(s)} i_{12} = 0 \\ M_{32} n_s \eta_{23}^{(c)} + M_{23}\eta_{23}^{(s)} i_{23} = 0 \\ M_{62}\eta_{26}^{(c)} + M_{26}\eta_{26}^{(s)} i_{26} = 0 \\ M_{72}\eta_{27}^{(c)} + M_{27}\eta_{27}^{(s)} i_{27} = 0 \\ M_{43}\eta_{34}^{(c)} + M_{34}\eta_{34}^{(s)} i_{34} n_s = 0 \\ M_{53}\eta_{35}^{(c)} + M_{35}\eta_{35}^{(s)} i_{35}\, n_s = 0 \\ M_{84}\eta_{48}^{(c)} + M_{48}\eta_{48}^{(s)} i_{48} = 0 \\ M_{95}\eta_{59}^{(c)} + M_{59}\eta_{59}^{(s)}\, i_{59} = 0 \end{cases}, \tag{59}$$

Note that the certain view of equation system Eq. (59) depends on states of power flows passing through the differential as well as through the clutches. For each pair of $k = \{1, 2, 3, 3\}$ and $l = \{2, 3, 4, 5\}$, possible states are switched simultaneously since these parts are being connected in the whole mechanism. Thus,

$$\begin{gathered} \boldsymbol{\eta}_G^{(s)} \in \{\boldsymbol{\eta}_G^{(d)}, \ \boldsymbol{\eta}_G^{(r)}\}, \qquad \boldsymbol{\eta}_G^{(c)} \in \{\boldsymbol{\eta}_G^{(r)}, \ \boldsymbol{\eta}_G^{(d)}\} \\ \boldsymbol{\eta}_G^{(d)} = \boldsymbol{\eta}_G \Rightarrow \boldsymbol{\eta}_G^{(r)} = \{\mathbf{1}\}, \qquad \boldsymbol{\eta}_G^{(r)} = \boldsymbol{\eta}_G \Rightarrow \boldsymbol{\eta}_G^{(d)} = \{\mathbf{1}\} \end{gathered} \tag{60}$$

where $\boldsymbol{\eta}_G$ – gearing efficiency vector with η_{kl}, $\{\mathbf{1}\}$ – vector of ones with the same size as $\boldsymbol{\eta}_G$.

Preprints (www.preprints.org) | NOT PEER-REVIEWED | Posted: 26 November 2021 doi:10.20944/preprints202111.0507.v1

Unlike the aforesaid, the clutches' elements can be in active and passive phases depending on values of friction moments M_{86} and M_{97} regardless of the basic mechanism state. A clutch may be withdrawing some torque from the carrier as well as returning it back. For each pair of $k = \{6, 7, 8, 9\}$ and $l = \{2, 2, 4, 5\}$ the state may be determined by the sign of the difference in moments since an angular velocity is the same at the both sides of an element

$$|M_{kl}| - |M_f| > 0 \tag{61}$$

where the friction moment $M_f = \{M_{86}, M_{97}\}$ for corresponding indexes k and l.

If the inequality Eq. (61) for a clutch component is satisfied, its mode will be "direct" and vice versa. This implies the following assertions, where upper indexes denote conditionally direct (d) and reverse (r) states.

$$\eta_{kl}^{(s)} \in \left\{\eta_{kl}^{(d)}, \ \eta_{kl}^{(r)}\right\}, \ \ \eta_{kl}^{(c)} \in \left\{\eta_{kl}^{(d)}, \ \eta_{kl}^{(r)}\right\}$$
$$\eta_{kl}^{(d)} = \eta_{kl} \Longrightarrow \eta_{kl}^{(r)} = 1, \ \ \eta_{kl}^{(d)} = \eta_{kl} \Longrightarrow \eta_{kl}^{(r)} = 1 \tag{62}$$

The pairwise use of the moments in Eq (59) as well as their sequential pair arrangement in the vector $\boldsymbol{M}$ makes possible to separate the parts of active and reaction moments through the matrices $\boldsymbol{e}_r$ at gear ratios and $\boldsymbol{e}_m$ for output loads of dimension $m \times 2m$. Thus, in the matrix $\boldsymbol{e}_r$, the elements corresponding to the mesh nodes based on each row and each second column, starting from the first, are equal to 1, while other elements equal 0. The same procedure for forming the matrix $\boldsymbol{e}_m$ but starting from the second column.

Considering the foregoing, the system of Eq. (59) may be represented in the matrix form as follows:

$$\boldsymbol{e}_M \boldsymbol{M} = \boldsymbol{z} \tag{63}$$

where for the generalized state of power flows

$$\boldsymbol{e}_M = \left(\boldsymbol{H}_G^{(s)} diag(\boldsymbol{i}) \boldsymbol{e}_r + \boldsymbol{H}_G^{(c)} \boldsymbol{e}_m\right) diag(\boldsymbol{N}_s) \tag{64}$$

On the other hand, based on the system Eq. (58), all the moments of vector $\boldsymbol{M}$ can be expressed by the elements of vector $\boldsymbol{M}_D$. Considering Eq. (24), it can be derived for the generalized case

$$\boldsymbol{E}_M = \left(diag(\boldsymbol{N}_D)\right)^{-1} \left(\boldsymbol{e}_m - \left(\boldsymbol{H}_G^{(s)} diag(\boldsymbol{i})\right)^{-1} \boldsymbol{H}_G^{(c)} \boldsymbol{e}_r\right)^T \tag{65}$$

where $\boldsymbol{N}_D$ may be obtained by replacing elements 3 and 4 in the vector $\boldsymbol{N}_s$ with $1/n_s$ and 1, correspondingly.

Then,

$$\boldsymbol{M} = \boldsymbol{E}_M \boldsymbol{M}_D, \qquad \boldsymbol{e}_M \boldsymbol{E}_M \boldsymbol{M}_D = \boldsymbol{z} \tag{66}$$

Another step is regarding replacing M_{32} with expression based on M_{43} and M_{53}. An additional condition can be formed for the reason that the driving moments of the differential carrier and satellites lie in different planes as shown in Fig. 5e. Obviously, for a satellite

$$P_{32} + P_{34} + P_{35} = 0 \tag{67}$$

Preprints (www.preprints.org) | NOT PEER-REVIEWED | Posted: 26 November 2021 doi:10.20944/preprints202111.0507.v1

Multiplying by the radius R_{23} of force transmission through the satellite's axle and by the number of satellites, obtain

$$n_s P_{32} R_{23} + n_s P_{34} R_{23} + n_s P_{35} R_{23} = 0 \tag{68}$$

or

$$n_s M_{32} + n_s P_{34} R_3 \frac{R_{23}}{R_3} + n_s P_{35} R_3 \frac{R_{23}}{R_3} = 0$$

$$n_s M_{32} + n_s M_{34} i_{34} u_{24} + n_s M_{35} i_{35} u_{25} = 0 \tag{69}$$

where $u_{24} = R_{23}/R_4$, $u_{25} = R_{23}/R_5$ – ratio of passing forces between the radii of satellites' axles and gearings (is may be accepted that $u_{24} = u_{25} = 1$).

Using Eq. (59), Eq. (69) can be rewritten in the generalized form, respectively

$$M_{32} \frac{\eta_{23}^{(c)} n_s}{\eta_{23}^{(s)} i_{23}} = M_{43} \frac{\eta_{34}^{(c)}}{\eta_{34}^{(s)}} + M_{53} \frac{\eta_{35}^{(c)}}{\eta_{35}^{(s)}} \tag{70}$$

Denote

$$b_{43} = \frac{\eta_{34}^{(c)}}{\eta_{34}^{(s)}} \frac{\eta_{23}^{(s)} i_{23}}{\eta_{23}^{(c)} n_s}, \quad b_{53} = \frac{\eta_{35}^{(c)}}{\eta_{35}^{(s)}} \frac{\eta_{23}^{(s)} i_{23}}{\eta_{23}^{(c)} n_s} \tag{71}$$

Then,

$$M_{32} = M_{43} b_{43} + M_{53} b_{53} \tag{72}$$

The latter allows to exclude the redundant variable M_{32} from $\boldsymbol{M}_D$ and reduce unknown variables. Denote transition matrix $\boldsymbol{S}$ and vector $\boldsymbol{M}_U$ of independent internal moments. Then

$$\boldsymbol{S} = \begin{pmatrix} 1 & 0 & 0 & 0 & 0 & 0 & 0 \\ 0 & 0 & 0 & b_{43} & b_{53} & 0 & 0 \\ 0 & 1 & 0 & 0 & 0 & 0 & 0 \\ 0 & 0 & 1 & 0 & 0 & 0 & 0 \\ 0 & 0 & 0 & 1 & 0 & 0 & 0 \\ 0 & 0 & 0 & 0 & 1 & 0 & 0 \\ 0 & 0 & 0 & 0 & 0 & 1 & 0 \\ 0 & 0 & 0 & 0 & 0 & 0 & 1 \end{pmatrix}, \quad \boldsymbol{M}_U = \begin{pmatrix} M_{21} \\ M_{62} \\ M_{72} \\ M_{43} \\ M_{53} \\ M_{84} \\ M_{95} \end{pmatrix}, \quad \boldsymbol{M}_D = \boldsymbol{S}\boldsymbol{M}_U \tag{73}$$

4.6. Matrix form

Thus, summarizing all the foregoing, the systems of Eqs. (15, 50, 59) can be rewritten in the matrix form as

$$\begin{cases} \boldsymbol{I}_D \boldsymbol{E}_\varepsilon \boldsymbol{\varepsilon}_D + \boldsymbol{E}_D \boldsymbol{E}_M \boldsymbol{M}_D = \boldsymbol{T}_D + \boldsymbol{V}_D \\ \boldsymbol{e}_\varepsilon \boldsymbol{E}_\varepsilon \boldsymbol{\varepsilon}_D = \boldsymbol{z}_m \\ \boldsymbol{e}_M \boldsymbol{E}_M \boldsymbol{M}_D = \boldsymbol{z}_m \end{cases} \tag{74}$$

where $\boldsymbol{z}_m$ – vector of zeros with dimension $m \times 1$.

Denote matrices for Eq. (74)

$$\boldsymbol{D} = \begin{pmatrix} \boldsymbol{I}_D & \boldsymbol{E}_D \\ \boldsymbol{e}_\varepsilon & \boldsymbol{Z}_{m,2m} \\ \boldsymbol{Z}_{m,n} & \boldsymbol{e}_M \end{pmatrix}, \ \boldsymbol{F} = \begin{pmatrix} \boldsymbol{E}_\varepsilon & \boldsymbol{Z}_{n,m} \\ \boldsymbol{Z}_{2m,2} & \boldsymbol{E}_M \end{pmatrix}, \ \boldsymbol{G} = \begin{pmatrix} \boldsymbol{E}_{2,2} & \boldsymbol{Z}_{2,m-1} \\ \boldsymbol{Z}_{m,2} & \boldsymbol{S} \end{pmatrix}, \ \boldsymbol{R} = \begin{pmatrix} \boldsymbol{T}_D + \boldsymbol{V}_D \\ \boldsymbol{z}_m \\ \boldsymbol{z}_m \end{pmatrix} \tag{75}$$

where $\boldsymbol{Z}_{q,r}$ – matrix of zeros with dimension $q \times r$, $\boldsymbol{E}_{2,2}$ – identity matrix 2×2.

Preprints (www.preprints.org) | NOT PEER-REVIEWED | Posted: 26 November 2021 doi:10.20944/preprints202111.0507.v1

According to the properties of Eqs. (55, 66), the kinematic and gearing equations in Eq. (74) become zeros, and, therefore, may be reduced by the rectangular identity matrix $\boldsymbol{E}_U$ with dimension $n \times n+2m$. Consequently, the final view of matrix components may be found as follows

$$\boldsymbol{x} = \begin{pmatrix} \boldsymbol{\varepsilon}_D \\ \boldsymbol{M}_U \end{pmatrix}, \quad \boldsymbol{E}_U = \boldsymbol{E}_{n,n+2m}, \quad \boldsymbol{B} = \boldsymbol{E}_U \boldsymbol{R}, \quad \boldsymbol{A} = \boldsymbol{E}_U \boldsymbol{D}\boldsymbol{F}\boldsymbol{G}, \quad \boldsymbol{x} = \boldsymbol{A}^{-1}\boldsymbol{B} \tag{76}$$

5. Simulation

5.1. Simulink-model

Based on the preceding theoretical expressions, a simulation model (Fig. 6) of the sport differential mechanism and its control under external loads conditions can be composed using MATLAB software (2021). The model's basic element is block *1 - System of differential Equations* containing a description code of differential equations for translationally and rotationally moving design parts. The block has complex input and output ports transmitting information through buses. In block *2 - Bus*, the required data about the model components' states are updated, and vectors of initial conditions for integrators and delay blocks are distributed.

Block *3 - Bus Selector* expands the complex output by the corresponding signal names. Namely, signals denote: *<PrevNormForces>* is a row vector of compression forces in friction clutches from previous integration step, *<InternalMoments>* is a vector of internal moments used for detecting clutches' operating modes and states of transmitting elements, *<ClutchActivation>* is a row vector of frictional couplings 6-8 and 7-9 modes taking values *0* - inactive and *1* - activated, *<PowerDirection>* - direction of the external power flow for the differential mechanism (*1* - direct, *-1* - reverse), *<AngularSpeeds>* - column vector of angular velocities according to Eq. (43), *<FrictionMoments>* is a row vector of frictional moments' values, *<Variable>* - a reserve variable for displaying any other data while testing the model, *<PistonDerivs>* - derivatives of hydraulic (translational elements) clutches' states, *<DifferDerivs>* - derivatives of the differential (rotational) components' states. All the needed information about the differential components' physical and geometric characteristics is collected in the *SDDms* structure and transmitted through block *4 - Sport Differential Data*.

In block *5 - Pressure*, initial control signals for hydraulic cylinders 10 and 11 are formed, followed by combining in a row vector in block *6 - Vector Concatenate*. Similarly, in block *7 - Torques* the external loads on the differential's shafts 1, 4, 5 are generated to be combined into a column vector in block *8 - Vector Concatenate*. The model uses two independent integrators: *9 - Differential Mechanism Integrator* for the rotational motion equations and *10 - Piston Integrator* for the equations of pistons' translational motion. Blocks *11 - Nf* and *12 - M* allow storing in memory the vectors of compression forces and internal moments at the previous

Preprints (www.preprints.org) | NOT PEER-REVIEWED | Posted: 26 November 2021 doi:10.20944/preprints202111.0507.v1

computing step. Block *13 - Results* accumulates the primary output data for analysis.

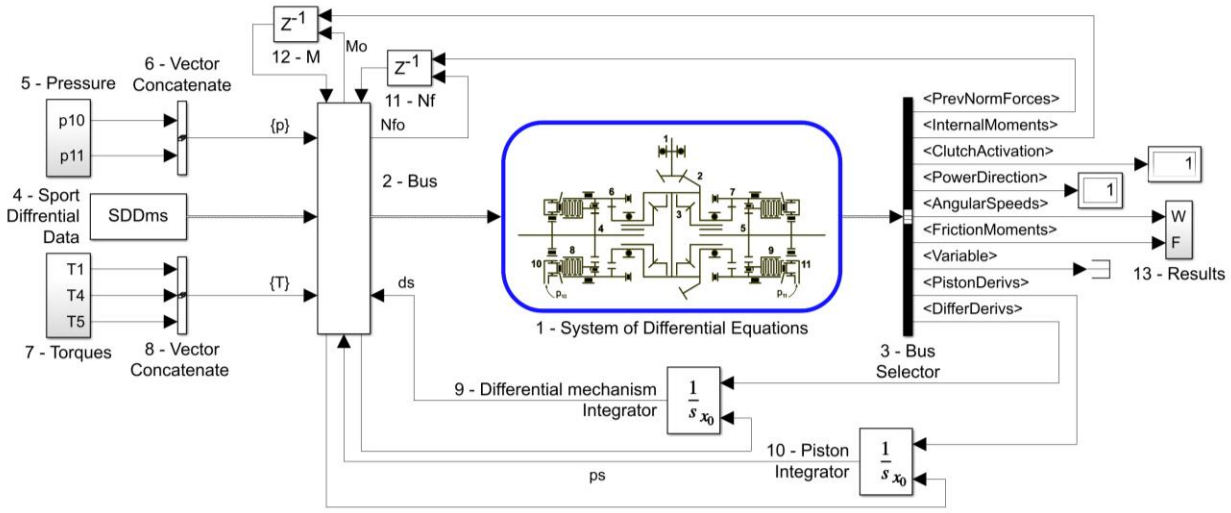

Figure 6. Simulink-model of the sport differential functioning

5.2. Testing the differential model operability

First of all, the model of DM itself must be tested. It is expected that the distribution of angular speeds, in this case, corresponds to the concept of "least resistance" for a power flow. Thus, the most general test mode may be formed using periodical loads with the same phases but different amplitudes (Fig. 7, External torque) on the mechanism shafts. The primary output information is the values of angular velocities of all the mechanism's rotating components. In turn, it can be stated that the shapes of the angular speeds' curves for shafts 1, 4, 5 are in good coordination, reflecting trends of the corresponding external torques. The internal moments' curves also inherit the nature of the external ones with distinctive step shifts when the power flow direction is changed. The solution's periodicity remains, which indicates the model stability. The main point implies that an axle with lower loading torque tends to have a higher angular speed, typical for symmetrical frictionless differentials.

Preprints (www.preprints.org) | NOT PEER-REVIEWED | Posted: 26 November 2021 doi:10.20944/preprints202111.0507.v1

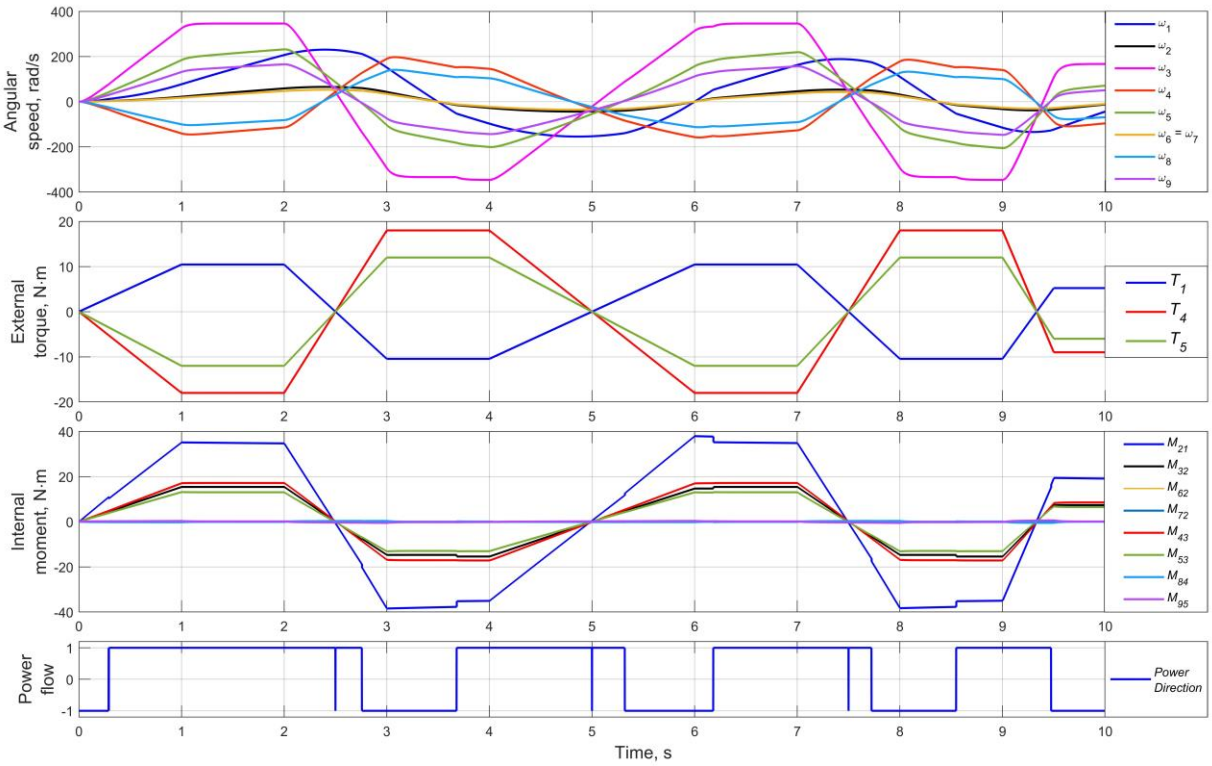

Figure 7. Modeling the mode of a conventional inter-axle differential

Consider now an option of activating one of the differential's clutches (Fig. 8) for the same external loading conditions as in Fig. 7. Proceeding from the fact that a larger external resistance torque passes through axle 4, the pressure increase p_{10} can be set while p_{11} remains zero (Fig. 8, Pressure). Reflect only ω_4 and ω_5 angular speeds as the output. The pressure increase phases are accompanied by the friction torque M_{86} ($M_{97} = 0$ because of $p_{11} = 0$). In the phase of positive values, this friction torque adds power to shaft 4 with a larger load, causing its angular speed ω_4 to exceed the ω_5 one, unlike the situation in Fig. 7. The internal moments M_{62} and M_{84} appear in the opposite phase, revealing their possible leading/driven states when the clutch 6-8 is activated. Thus, in contrast to the situation in Fig. 7, both torque and speed output parameters are redistributed, and the angular speed of a more loaded shaft can exceed one of a less loaded shaft.

Preprints (www.preprints.org) | NOT PEER-REVIEWED | Posted: 26 November 2021 doi:10.20944/preprints202111.0507.v1

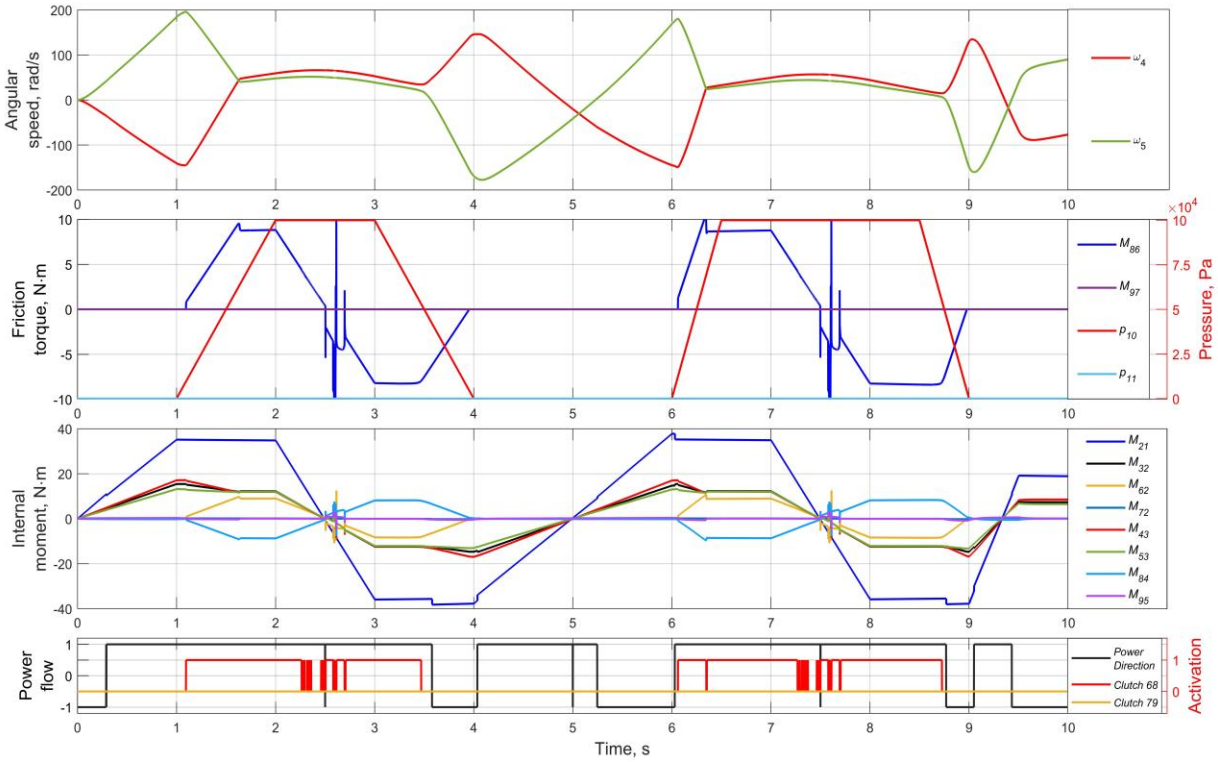

Figure 8. Modeling the mode of activating the clutch 6-8

5.3. The case of zero resistance

The case when one of the differential's output axles is unloaded (or the load tends to zero) is particularly interesting. Such a situation typically occurs due to the lack of tire-road adhesion on one of the same axle wheels. In the case of a conventional symmetrical differential, all the power goes to drive the wheel with the worst adhesion conditions, and its angular speed tends to a maximum. In the case of an active limited-slip differential, a part of the carrier's torque may be transmitted to a lagging axle, maintaining the differences in the angular speeds. These variants' properties can be compared with the example in Fig. 9. Thus, axle 5 is unloaded, and the torques on shafts 1 and 4 are constant.

As seen, outside the time moments of activating the clutch 6-8, the angular speed of the unloaded axis 5 rapidly increases, and axis 4 rotates in the opposite direction under the influence of a negative load, which corresponds to the operational mode of a conventional differential. However, in the periods 1.5-3.5 s and 6.5-8-5 s of stable pressure in the clutch's 6-8 cylinder, the angular speed ω_4 of the loaded shaft even slightly exceeds the angular speed ω_5. At the same time, the moment M_{43} value of the side gear 4 falls to a minimum, while the moments M_{62} and M_{84} reach their maximum modules. This situation corresponds to transmitting the maximum torque through one output shaft. Thus, the wheels' angular speeds are synchronized along with ensuring maximum vehicle passability.

Preprints (www.preprints.org) | NOT PEER-REVIEWED | Posted: 26 November 2021 doi:10.20944/preprints202111.0507.v1

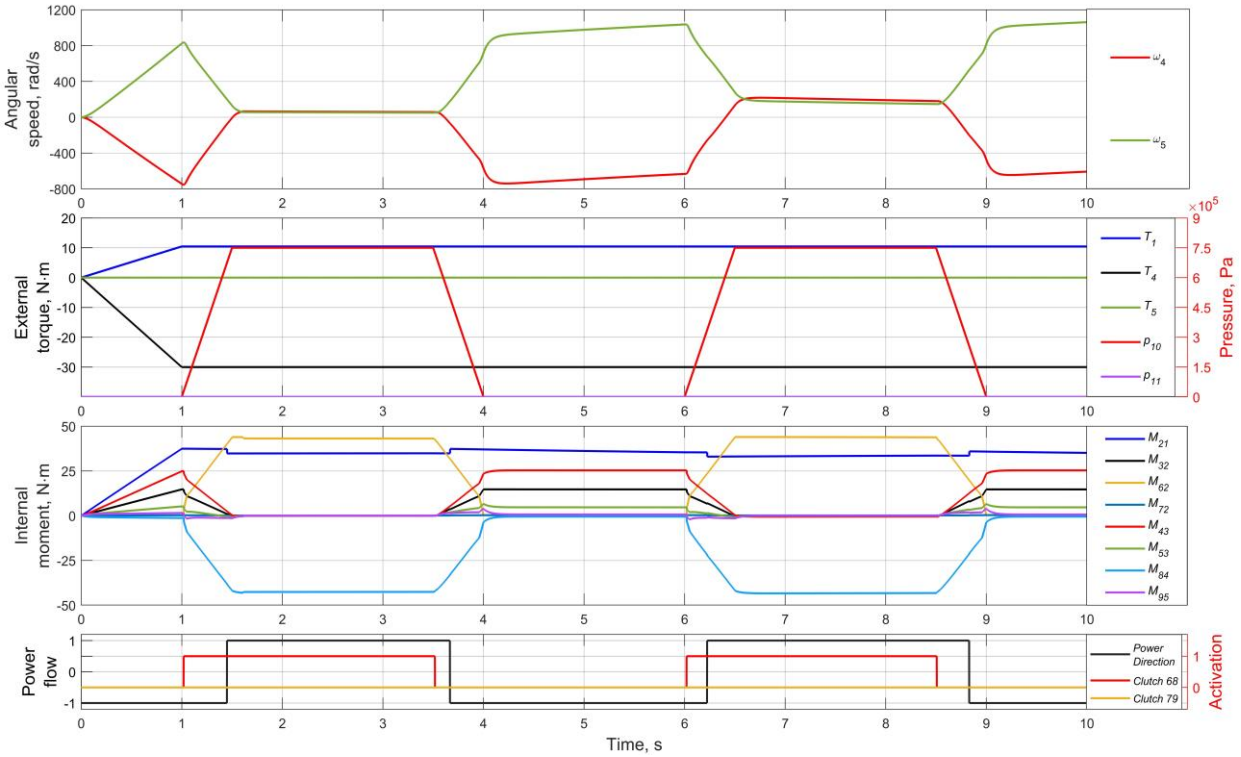

Figure 9. Simulation of transmitting all the torque through one output axle

5.4. Alternating activation

The following example shows the alternating actuation of the friction clutches. This option can be used when correcting the trajectory under conditions of a motion track with a variable sign periodic curvature. Suppose the resisting moments to be changed periodically, and the driving moment is constant, as shown in Fig. 10. At the same time, the load moments are alternately changed to larger/smaller amplitude values. A conventional differential design would result in a higher angular speed on the shaft with less load and vice versa. The activation of the friction clutches to be organized in such a way to match the increase of axles' loads. As an immediate result, only the angular velocities ω_4 and ω_5 are taken accompanied with piston strokes x_{p10}, x_{p11}. As seen, the activation of corresponding clutches causes the angular speed rise for a semi-axle under higher load conditions, which allows more torque to be transmitted to a wheel with better adhesion conditions, ensuring a greater reaction value (traction force).

Preprints (www.preprints.org) | NOT PEER-REVIEWED | Posted: 26 November 2021 doi:10.20944/preprints202111.0507.v1

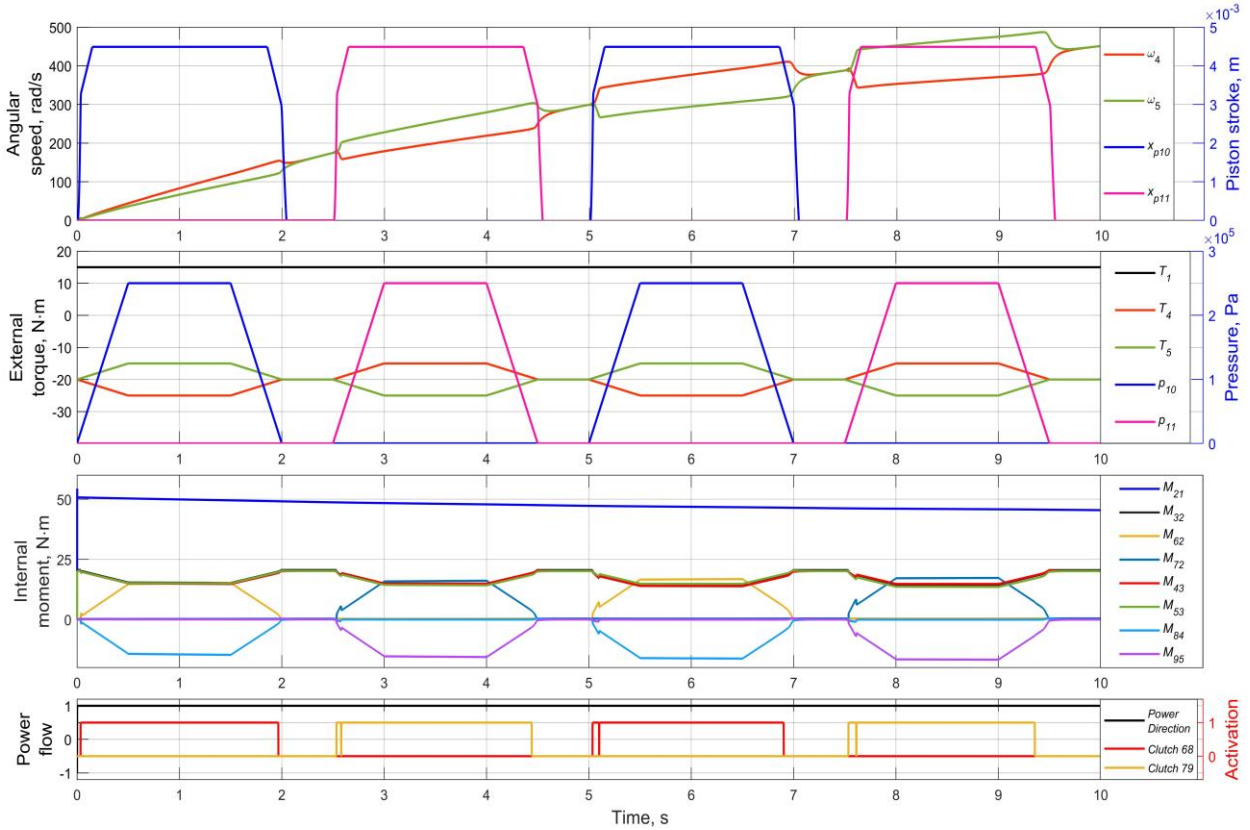

Figure 10. Simulation of alternating activation of friction clutches

5.5. Analysis of results

A few comments are to be made about the data used and its impact on the simulation results. First, the question concerns the moments of friction forces and their influence on the solution accuracy. Varying the data has shown that the friction torque's increased sensitivity relative to the cylinder pressure negatively affects the slip smoothness. Thus, the variant of "hard" friction disks leads to the appearance of jerks and solution instability. The decreased sensitivity requires a larger pressure value and may lead to a delay in the response time of a controlling drive. Thus, the compromise must meet the demands of operating properties and design compactness. Note that a decrease in the friction coefficient for clutches and an increase in the number of frictional pairs positively affect smoothing the torque passing from the differential's carrier. This issue can be also facilitated by introducing a piecewise constant compressing stiffness of a clutch package up to a deformation limit. Thus, the adjustment and tuning of this design simulation model compose a separate task for adapting the model functioning to a specific range of loads and vehicle motion modes.

6. Conclusions

Based on this study, two main conclusions are made. The first is related to obtaining the essential effect from forcibly redistributing the torque using the sport differential technology. All simulations carried out with different sets of initial conditions confirm the model's efficiency in transmitting larger torque to an axle with higher resistance and equalizing the angular speeds of

output shafts in contrast to the principle of functioning the conventional (open) and passive limited-slip differentials. The angular speed growth on a shaft with higher resistance leads to an increase in slip (up to a critical) and, as a rule, to a rise in traction force on a wheel, which contributes to the appearance of an additional turning moment relative to the vehicle vertical axis (Fig. 2). At the same time, the friction clutch usage can be practical not only in the traction mode but also in the driven one, when due to the activation of the outer wheel clutch, the negative longitudinal reaction decreases. This fosters the wide use of various algorithms for controlling the sport differential to stabilize/align the vehicle trajectory. In addition, the possibility of transmitting all the torque to one of the output axles was demonstrated to maintain the vehicle passability in conditions of limited road-tire adhesion. Thus, the proposed sport differential model can be used for simulating the active control vehicle transmissions.

The second conclusion concerns the proposed alternative method for obtaining differential equations that describe the dynamics of rotational mechanical systems. As demonstrated, the main idea consisted of decomposing a mechanical system onto elementary components with the independent formation of three equations: dynamics, kinematic constraints, and force interactions. All the internal efforts' signs are determined automatically. The developed mathematical apparatus effectively reduces the total number of equations for compactness and lowers the simulation time. Thus, the approach itself corresponds to the modern trend of multibody modeling and provides a field for developing a technique to automate the composition of motion equations for mechanical systems. The proposed method is supposed to be further improved in the complex modeling of all-wheel-drive transmissions with several DMs.

Funding. This research is financially supported by NSERC (Natural Sciences and Engineering Research Council) Canada.

Acknowledgements. Authors are grateful to Mathworks company for the access to MATLAB software based on Ryerson University's license.

Author Contributions. Conceptualization, M.D. and S.E.; Methodology, M.D.; Software, M.D.; Validation, M.D. and S.E.; Formal Analysis, S.E.; Investigation, M.D.; Resources, S.E.; Data Curation, M.D.; Writing – Original Draft Preparation, M.D.; Writing – Review & Editing, S.E.; Visualization, M.D.; Supervision, S.E.; Project Administration, S.E.; Funding Acquisition, S.E.

Conflict of Interest. The authors declare no conflict of interest.

References

Annicchiarico, C., Rinchi, M., Pellari, S., Capitani, R. (2014). Design of a Semi Active Differential to Improve the Vehicle Dynamics. *Proceedings of the ASME 2014 12th Biennial Conference on Engineering Systems Design and Analysis*. *Volume 1.* Copenhagen, Denmark. July 25-27. V001T02A006. ASME. https://doi.org/10.1115/ESDA2014-20157

Assadian F., Hancock M., Best, M. (2008). Development of a control algorithm for an active limited slip differential. Loughborough University. Conference contribution. https://hdl.handle.net/2134/8324

Audi Sport Differential, (2021). https://www.audi-mediacenter.com/en/40-years-of-quattro-the-all-conquering-technology-from-audi-12598/the-mechanical-quattro-systems-12602 (accessed 07.08.2021)

Audi Sport Differential Technology, (2021). https://www.youtube.com/watch?v=FwhrmFuov-4 (accessed 12.08.2021)

Brumercik, F., Lukac, M., Nieoczym, A. (2015). Mechanical differential mathematical model. Komunikacie. 17. 88-91.

Chen, Y.-F., Chen, I.-M., Chang, J., Liu, T. (2017(1)). Design and Analysis of a New Torque Vectoring System with a Ravigneaux Gearset for Vehicle Applications. Energies, 10, 2157. https://doi.org/10.3390/en10122157.

Chen, Y.-F., Hsu, H.-C., Yang, C.-P., Liu, T. (2017(2)). Design and Modeling of a Novel Torque Vectoring Differential System. MATEC Web of Conferences. 108. 07004. 10.1051/matecconf/201710807004.

Deur, J., Ivanovic, V., Hancock, M., Assadian, F. (2010). Modeling and Analysis of Active Differential Dynamics. *Journal of Dynamic Systems Measurement and Control-transactions of The Asme*, *132*, 061501.

Forstinger M., Bauer R., Hofer A. (2015). Modelling and Simulation of Passive Limited-slip Differentials. IFAC-PapersOnLine, Volume 48, Issue 1, Pages 502-507, ISSN 2405-8963, https://doi.org/10.1016/j.ifacol.2015.05.057

Gadola, M., Chindamo, D. (2018). The Mechanical Limited-Slip Differential Revisited: High-Performance and Racing Car Applications. International Journal of Applied Engineering Research ISSN 0973-4562 Volume 13, Number 2, pp. 1478-1495.

Jaafari, S. M. M., Shirazi, K. H. (2018). Integrated Vehicle Dynamics Control Via Torque Vectoring Differential and Electronic Stability Control to Improve Vehicle Handling and Stability Performance. ASME. *J. Dyn. Sys., Meas., Control*. July 2018; 140(7): 071003.

Ji, J., Li, Y. W., Peng, H. (2011). Effects of Driveline and Tire Model on the Performance of Active Differential: Modeling and Simulation. In Applied Mechanics and Materials (Vols. 97-98, pp. 771-776). Trans Tech Publications, Ltd. https://doi.org/10.4028/www.scientific.net/amm.97-98.771

MATLAB R2021b. https://www.mathworks.com/ (access 24/10/2021)

Morselli R., Zanasi R., Sandoni G. (2006). Detailed and reduced dynamic models of passive and active limited-slip car differentials, Mathematical and Computer Modelling of Dynamical Systems, 12:4, 347-362, DOI: 10.1080/13873950500066959.

Russo R., Strano S., Terzo M. (2016). Enhancement of vehicle dynamics via an innovative magnetorheological fluid limited slip differential. Mechanical Systems and Signal Processing, Volumes 70-71, Pages 1193-1208, ISSN 0888-3270, https://doi.org/10.1016/j.ymssp.2015.09.029

Virlez G., Brüls O., Tromme E., Duysinx P. (2013). Modeling joints with clearance and friction in multibody dynamic simulation of automotive differentials, Theoretical and Applied Mechanics Letters, Volume 3, Issue 1. https://doi.org/10.1063/2.1301303

Virlez, G., Brüls, O., Duysinx, P., Poulet, N. (2011). Simulation of Differentials in Four-Wheel Drive Vehicles Using Multibody Dynamics. Proceedings of the ASME Design Engineering Technical Conference. 4. 10.1115/DETC2011-48313.